Published OnlineFirst March 23, 2011; DOI:10.1158/1078-0432.CCR-11-0063

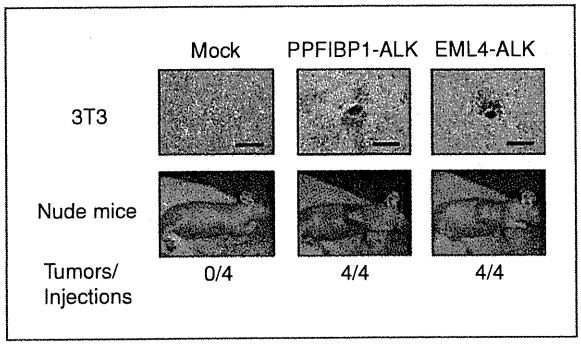

Figure 4. Transforming potential of PPFIBP1–ALK. Top, mouse 3T3 fibroblasts were infected with retroviruses encoding PPFIBP1–ALK or EML4–ALK or with the corresponding empty virus (Mock). The cells were photographed after 14 days of culture. Scale bars, 400 μm. Bottom, Nude mice were injected subcutaneously with the corresponding 3T3 cells, and tumor formation was examined after 14 days. The number of tumors formed per 4 injections is indicated at the bottom.

the 3′-untranslated region of *ALK* mRNA (GenBank accession no. NM_004304), a full-length *PPFIBP1–ALK* cDNA of 2488 bp was successfully amplified, which should have produced a fusion kinase of 811 amino acids with a predicted molecular weight of 90,740 Da (Supplementary Fig. 1).

To examine the transforming potential of PPFIBP1–ALK, a recombinant ecotropic retrovirus was generated to express PPFIBP1–ALK, which was used to infect mouse 3T3 fibroblasts. As shown in Figure 4, PPFIBP1–ALK produced hundreds of transformed foci over 14 days of culture, which was comparable with the observation with EML4–ALK. Furthermore, subcutaneous injection of the infected 3T3 cells into the shoulder of nude mice revealed that those expressing either PPFIBP1–ALK or EML4–ALK formed large tumors *in vivo*.

Discussion

Since their discovery in 1994, appropriate diagnosis of ALK fusion-positive tumors with conventional anti-ALK immunohistochemistry methods has been accepted. However, EML4–ALK in lung adenocarcinoma, identified in 2007, did not stain positive for ALK with conventional immunohistochemistry methods (21, 35). We developed a sensitive immunohistochemistry method, the iAEP method, and successfully stained EML4–ALK with ordinary anti-ALK mouse monoclonal antibodies (21, 31–33). Such observation further indicates a possibility that staining cancer specimens with sensitive immunohistochemical methods (such as iAEP) may detect novel ALK fusions in the "ALK-negative" tumors defined by conventional anti-ALK immunohistochemistry methods. On the basis of this hypothesis, we have identified a novel ALK fusion in "ALK-negative" IMT.

Caution is needed in practical settings. For example, rhabdomyosarcoma, especially of the alveolar type, often expresses wild-type ALK at a detectable level with conventional anti-ALK immunohistochemistry (40). Moreover, in our experience, a small portion of small cell carcinoma and large cell endocrine carcinoma of the lung, and some sarcomas, may be positive for ALK by iAEP immunohistochemistry, expressing wild-type ALK. Therefore, in order to specifically detect ALK fusions with sensitive anti-ALK immunohistochemistry, a confirmatory test by using FISH, RT-PCR, or similar is usually required. If a tumor is positive for a confirmatory test and the suspected partner gene is not a reported one, 5′-RACE or inverse reverse transcriptase PCR methods can be used for the identification of the suspected partner. Even if overexpressed, wild-type ALK may not be oncogenic (20, 21, 37, 38), although some investigators have suggested that wild-type ALK overexpression above a certain threshold level drives the growth of neuroblastoma (41). Further investigation will be required to clarify if wild-type ALK overexpression is a target for ALK inhibitor therapy.

IMT is a rare mesenchymal tumor that has been referred to as inflammatory pseudotumor, plasma cell granuloma, fibroxanthoma, fibrous histiocytoma, pseudosarcomatous myofibroblastic tumor, and invasive fibrous tumor of the tracheobronchial tree (42). It occurs in the soft tissues as well as in the viscera and the lung, and is more likely to occur in children and young adults. Histologically, IMT is composed of a variable admixture of bland, spindle-shaped myofibroblast-like cells and an inflammatory component of lymphocytes, eosinophils, plasma cells, and macrophages. Recent genetic studies have elucidated clonal chromosomal abnormality involving 2p23, at which ALK is located, in a subset of IMT. The expression of ALK fusion proteins is detected by anti-ALK immunohistochemistry in approximately 50% of IMT cases (42), in which various ALK fusion genes have been reported (Table 1). Collectively, these lines of evidence support ALK-positive IMT being a distinct neoplastic entity. However, the other 50% of IMT cases are negative for anti-ALK immunohistochemistry, and thus in terms of pathogenesis it remains unknown whether these ALK-negative IMTs should be included in the same entity or not. In fact, 1 ALK-negative IMT case did not respond to crizotinib therapy (29). However, we have detected a novel ALK-fusion in "ALK-negative" IMT that subsequently proved positive for ALK with the iAEP immunohistochemistry method. Therefore, unexpectedly lowly expressed ALK fusions may explain the pathogenesis of a portion of "ALK-negative" IMT cases. PPFIBP1–ALK represents such an ALK fusion, although we do not yet know what proportion of "ALK-negative" IMTs can be attributed to this novel subtype. "ALK-negative" IMT warrants screening with the iAEP method to detect this fusion or other, unrecognized, ALK fusions.

PPFIBP1 codes liprin beta 1 (also called PTPRF-interacting protein-binding protein 1). This 114 kDa protein is a member of the leukocyte common antigen–related (LAR) transmembrane tyrosine phosphatase-interacting protein family that may regulate LAR protein properties via interaction with another member of the family, liprin alpha1 (43). Liprin beta 1 expresses in intestinal lymphatic endothelial cells *in vitro* and lymphatic vasculature *in vivo*,

Published OnlineFirst March 23, 2011; DOI:10.1158/1078-0432.CCR-11-0063

Table 1. ALK fusion partners in well-documented IMT cases

Partner	Locus	Age	Sex	Site	Year, First author
TPM3	1p23	30	F	Lung	2000, Lawrence
		23	F	Abdomen	2000, Lawrence
		4	M	Lung	2006, Yamamoto
		29	F	Ileum	2006, Milne
		4	M	Lung	2007, Kinoshita
TPM4	19p13	1	M	Abdomen	2000, Lawrence
		6	M	Mesentery	2003, Hisaoka
		25	M	Prostate	2003, Hisaoka
		5	M	Mesentery	2006, Yamamoto
		5	F	Urinary bladder	2006, Yamamoto
CLTC	17q23	3	F	Neck	2001, Bridge
		37	M	Pelvis	2001, Bridge
		2	M	Thoracic cavity	2006, Yamamoto
		6	M	Mesentery	2006, Yamamoto
		0	F	Mediastinum	2007, Patel
CARS	11p15	0	M	Abdomen	2002, Cools
		10	M	Neck	2003, Debelenko
RANBP2	2q13	7	M	Abdomen	2003, Ma
		0	M	Abdomen	2003, Ma
		2	M	Abdomen	2007, Patel
		34	M	Liver	2008, Chen
		44	M	Abdomen	2010, Butrynski
ATIC	2q35	46	M	Urinary bladder	2003, Debiec-Rychter
SEC31L1	4q21	23	M	Abdomen	2006, Panagopoulos
PPFIBP1	12p11	45	M	Lung	Present case 1
		34	F	Lung	Present case 2

and plays an important role in the maintenance of lymphatic vessel integrity in *Xenopus* tadpoles (44). PPFIBP1 has 5 coiled-coil domains in exons 5 through 12, and the upper 3 domains are conserved in fusion form with ALK (Fig. 2D). The coiled-coil domain is shared in all ALK fusion partners (except for NPM, MSN, and SQSTM1), with which the ALK fusion proteins homodimerize leading to constitutive activation of ALK kinase domains (8, 19). As expected, in the present study, the oncogenicity of PPFIBP1–ALK was clearly confirmed with an *in vitro* focus formation assay and an *in vivo* tumorigenicity assay.

The difference in subcellular localization has contributed to the discovery/identification of various ALK fusions. Likewise, the difference in the expression level found is here proved important in the accurate detection of fusion proteins. Sensitive immunohistochemical methods such as iAEP will broaden the potential value of immunohistochemistry, which is a simple and long-established histopathologic technique in the fields of research and diagnosis. The ALK positivity rate (approximately 50%) in IMT should be reassessed with these more sensitive methods, possibly leading to the identification of novel ALK fusions and more candidates for ALK inhibitor therapy. A novel ALK fusion, VCL–ALK, has recently been identified in renal cancers (45, 46). In addition to IMT, therefore, a reassessment of diverse "ALK-negative" human cancers may be required in the forthcoming era of ALK inhibitor therapy.

Disclosure of Potential Conflicts of Interest

K. Takeuchi, scientific advisor for developing an anti-ALK iAEP immunohistochemistry kit (ALK Detection Kit, Nichirei Bioscience, Japan) and in charge of pathology screening for ALK fusions using the immunohistochemistry kit and an original probe set for ALK split FISH assay in a clinical trial of an ALK inhibitor (AF802, Chugai, Japan). The other authors disclosed no potential conflicts of interest.

Grant Support

This work was supported in part by Grants-in-Aid for Scientific Research from the Ministry of Education, Culture, Sports, Science, and Technology of Japan as well as by grants from the Japan Society for the Promotion of Science; the Ministry of Health, Labor, and Welfare of Japan; the Vehicle Racing Commemorative Foundation of Japan; Princess Takamatsu Cancer Research Fund; and the Uehara Memorial Foundation.

The costs of publication of this article were defrayed in part by the payment of page charges. This article must therefore be hereby marked *advertisement* in accordance with 18 U.S.C. Section 1734 solely to indicate this fact.

Received January 9, 2011; revised March 7, 2011; accepted March 15, 2011; published OnlineFirst March 23, 2011.

Published OnlineFirst March 23, 2011; DOI:10.1158/1078-0432.CCR-11-0063

References

1. Morris SW, Kirstein MN, Valentine MB, Dittmer KG, Shapiro DN, Saltman DL, et al. Fusion of a kinase gene, ALK, to a nucleolar protein gene, NPM, in non-Hodgkin's lymphoma. Science 1994; 263:1281–4.
2. Shiota M, Fujimoto J, Semba T, Satoh H, Yamamoto T, Mori S. Hyperphosphorylation of a novel 80 kDa protein-tyrosine kinase similar to Ltk in a human Ki-1 lymphoma cell line, AMS3. Oncogene 1994;9:1567–74.
3. Lamant L, Dastugue N, Pulford K, Delsol G, Mariame B. A new fusion gene TPM3-ALK in anaplastic large cell lymphoma created by a (1;2)(q25;p23) translocation. Blood 1999;93:3088–95.
4. Meech SJ, McGavran L, Odom LF, Liang X, Meltesen L, Gump J, et al. Unusual childhood extramedullary hematologic malignancy with natural killer cell properties that contains tropomyosin 4–anaplastic lymphoma kinase gene fusion. Blood 2001;98:1209–16.
5. Colleoni GW, Bridge JA, Garicochea B, Liu J, Filippa DA, Ladanyi M. ATIC-ALK: A novel variant ALK gene fusion in anaplastic large cell lymphoma resulting from the recurrent cryptic chromosomal inversion, inv(2)(p23q35). Am J Pathol 2000;156:781–9.
6. Hernández L, Pinyol M, Hernández S, Beà S, Pulford K, Rosenwald A, et al. TRK-fused gene (TFG) is a new partner of ALK in anaplastic large cell lymphoma producing two structurally different TFG-ALK translocations. Blood 1999;94:3265–8.
7. Touriol C, Greenland C, Lamant L, Pulford K, Bernard F, Rousset T, et al. Further demonstration of the diversity of chromosomal changes involving 2p23 in ALK-positive lymphoma: 2 cases expressing ALK kinase fused to CLTCL (clathrin chain polypeptide-like). Blood 2000;95:3204–7.
8. Tort F, Pinyol M, Pulford K, Roncador G, Hernandez L, Nayach I, et al. Molecular characterization of a new ALK translocation involving moesin (MSN-ALK) in anaplastic large cell lymphoma. Lab Invest 2001;81:419–26.
9. Lamant L, Gascoyne RD, Duplantier MM, Armstrong F, Raghab A, Chhanabhai M, et al. Non-muscle myosin heavy chain (MYH9): a new partner fused to ALK in anaplastic large cell lymphoma. Genes Chromosomes Cancer 2003;37:427–32.
10. Cools J, Wlodarska I, Somers R, Mentens N, Pedeutour F, Maes B, et al. Identification of novel fusion partners of ALK, the anaplastic lymphoma kinase, in anaplastic large-cell lymphoma and inflammatory myofibroblastic tumor. Genes Chromosomes Cancer 2002;34: 354–62.
11. Lawrence B, Perez-Atayde A, Hibbard MK, Rubin BP, Dal Cin P, Pinkus JL, et al. TPM3-ALK and TPM4-ALK oncogenes in inflammatory myofibroblastic tumors. Am J Pathol 2000;157:377–84.
12. Bridge JA, Kanamori M, Ma Z, Pickering D, Hill DA, Lydiatt W, et al. Fusion of the ALK gene to the clathrin heavy chain gene, CLTC, in inflammatory myofibroblastic tumor. Am J Pathol 2001;159:411–5.
13. Ma Z, Hill DA, Collins MH, Morris SW, Sumegi J, Zhou M, et al. Fusion of ALK to the Ran-binding protein 2 (RANBP2) gene in inflammatory myofibroblastic tumor. Genes Chromosomes Cancer 2003;37:98–105.
14. Debiec-Rychter M, Marynen P, Hagemeijer A, Pauwels P. ALK-ATIC fusion in urinary bladder inflammatory myofibroblastic tumor. Genes Chromosomes Cancer 2003;38:187–90.
15. Panagopoulos I, Nilsson T, Domanski HA, Isaksson M, Lindblom P, Mertens F, et al. Fusion of the SEC31L1 and ALK genes in an inflammatory myofibroblastic tumor. Int J Cancer 2006;118:1181–6.
16. Delsol G, Lamant L, Mariamé B, Pulford K, Dastugue N, Brousset P, et al. A new subtype of large B-cell lymphoma expressing the ALK kinase and lacking the 2; 5 translocation. Blood 1997;89:1483–90.
17. Gascoyne RD, Lamant L, Martin-Subero JI, Lestou VS, Harris NL, Müller-Hermelink HK, et al. ALK-positive diffuse large B-cell lymphoma is associated with Clathrin-ALK rearrangements: report of 6 cases. Blood 2003;102:2568–73.
18. Van Roosbroeck K, Cools J, Dierickx D, Thomas J, Vandenberghe P, Stul M, et al. ALK-positive large B-cell lymphomas with cryptic SEC31A-ALK and NPM1-ALK fusions. Haematologica 2010;95: 509–13.
19. Takeuchi K, Soda M, Togashi Y, Ota Y, Sekiguchi Y, Hatano S, et al. Identification of a novel fusion, SQSTM1-ALK, in ALK-positive large B-cell lymphoma. Haematologica 2010.
20. Soda M, Choi YL, Enomoto M, Takada S, Yamashita Y, Ishikawa S, et al. Identification of the transforming EML4-ALK fusion gene in non-small-cell lung cancer. Nature 2007;448:561–6.
21. Takeuchi K, Choi YL, Togashi Y, Soda M, Hatano S, Inamura K, et al. KIF5B-ALK, a novel fusion oncokinase identified by an immunohistochemistry-based diagnostic system for ALK-positive lung cancer. Clin Cancer Res 2009;15:3143–9.
22. Chan JK, Lamant L, Algar E, Delsol G, Tsang WY, Lee KC, et al. ALK+ histiocytosis: a novel type of systemic histiocytic proliferative disorder of early infancy. Blood 2008;112:2965–8.
23. Du XL, Hu H, Lin DC, Xia SH, Shen XM, Zhang Y, et al. Proteomic profiling of proteins dysregulted in Chinese esophageal squamous cell carcinoma. J Mol Med 2007;85:863–75.
24. Jazii FR, Najafi Z, Malekzadeh R, Conrads TP, Ziaee AA, Abnet C, et al. Identification of squamous cell carcinoma associated proteins by proteomics and loss of beta tropomyosin expression in esophageal cancer. World J Gastroenterol 2006;12:7104–12.
25. Rikova K, Guo A, Zeng Q, Possemato A, Yu J, Haack H, et al. Global survey of phosphotyrosine signaling identifies oncogenic kinases in lung cancer. Cell 2007;131:1190–203.
26. Lin E, Li L, Guan Y, Soriano R, Rivers CS, Mohan S, et al. Exon array profiling detects EML4-ALK fusion in breast, colorectal, and non-small cell lung cancers. Mol Cancer Res 2009;7:1466–76.
27. Chiarle R, Voena C, Ambrogio C, Piva R, Inghirami G. The anaplastic lymphoma kinase in the pathogenesis of cancer. Nat Rev Cancer 2008;8:11–23.
28. Kwak EL, Bang YJ, Camidge DR, Shaw AT, Solomon B, Maki RG, et al. Anaplastic lymphoma kinase inhibition in non-small-cell lung cancer. N Engl J Med 2010;363:1693–703.
29. Butrynski JE, D'Adamo DR, Hornick JL, Dal Cin P, Antonescu CR, Jhanwar SC, et al. Crizotinib in ALK-rearranged inflammatory myofibroblastic tumor. N Engl J Med 2010;363:1727–33.
30. Falini B, Bigerna B, Fizzotti M, Pulford K, Pileri SA, Delsol G, et al. ALK expression defines a distinct group of T/null lymphomas ("ALK lymphomas") with a wide morphological spectrum. Am J Pathol 1998;153:875–86.
31. Sakairi Y, Nakajima T, Yasufuku K, Ikebe D, Kageyama H, Soda M, et al. EML4-ALK fusion gene assessment using metastatic lymph node samples obtained by endobronchial ultrasound-guided transbronchial needle aspiration. Clin Cancer Res 2010;16:4938–45.
32. Nakajima T, Kimura H, Takeuchi K, Soda M, Mano H, Yasufuku K, et al. Treatment of lung cancer with an ALK inhibitor after EML4-ALK fusion gene detection using endobronchial ultrasound-guided transbronchial needle aspiration. J Thorac Oncol 2010;5:2041–3.
33. Jokoji R, Yamasaki T, Minami S, Komuta K, Sakamaki Y, Takeuchi K, et al. Combination of morphological feature analysis and immunohistochemistry is useful for screening of EML4-ALK-positive lung adenocarcinoma. J Clin Pathol 2010;63:1066–70.
34. Mino-Kenudson M, Chirieac LR, Law K, Hornick JL, Lindeman N, Mark EJ, et al. A novel, highly sensitive antibody allows for the routine detection of ALK-rearranged lung adenocarcinomas by standard immunohistochemistry. Clin Cancer Res 2010;16:1561–71.
35. Martelli MP, Sozzi G, Hernandez L, Pettirossi V, Navarro A, Conte D, et al. EML4-ALK rearrangement in non-small cell lung cancer and non-tumor lung tissues. Am J Pathol 2009;174:661–70.
36. Shiota M, Nakamura S, Ichinohasama R, Abe M, Akagi T, Takeshita M, et al. Anaplastic large cell lymphomas expressing the novel chimeric protein p80NPM/ALK: a distinct clinicopathologic entity. Blood 1995;86:1954–60.
37. Takeuchi K, Choi YL, Soda M, Inamura K, Togashi Y, Hatano S, et al. Multiplex reverse transcription-PCR screening for EML4-ALK fusion transcripts. Clin Cancer Res 2008;14:6618–24.
38. Choi YL, Takeuchi K, Soda M, Inamura K, Togashi Y, Hatano S, et al. Identification of novel isoforms of the EML4-ALK transforming gene in non-small cell lung cancer. Cancer Res 2008;68:4971–6.

Published OnlineFirst March 23, 2011; DOI:10.1158/1078-0432.CCR-11-0063

39. Onishi M, Kinoshita S, Morikawa Y, Shibuya A, Phillips J, Lanier LL, et al. Applications of retrovirus-mediated expression cloning. Exp Hematol 1996;24:324–9.
40. Pillay K, Govender D, Chetty R. ALK protein expression in rhabdomyosarcomas. Histopathology 2002;41:461–7.
41. Passoni L, Longo L, Collini P, Coluccia AM, Bozzi F, Podda M, et al. Mutation-independent anaplastic lymphoma kinase overexpression in poor prognosis neuroblastoma patients. Cancer Res 2009;69:7338–46.
42. Travis WD, Elisabeth B, Muller-Hermelink HK, Harris CC, editors. Pathology and Genetics of Tumours of the Lung, Pleural, Thymus and Heart. Lyon: IARC Press; 2004.
43. Kriajevska M, Fischer-Larsen M, Moertz E, Vorm O, Tulchinsky E, Grigorian M, et al. Liprin beta 1, a member of the family of LAR transmembrane tyrosine phosphatase-interacting proteins, is a new target for the metastasis-associated protein S100A4 (Mts1). J Biol Chem 2002;277:5229–35.
44. Norrmén C, Vandevelde W, Ny A, Saharinen P, Gentile M, Haraldsen G, et al. Liprin (beta)1 is highly expressed in lymphatic vasculature and is important for lymphatic vessel integrity. Blood 2010;115:906–9.
45. Debelenko LV, Raimondi SC, Daw N, Shivakumar BR, Huang D, Nelson M, et al. Renal cell carcinoma with novel VCL-ALK fusion: new representative of ALK-associated tumor spectrum. Mod Pathol 2010.
46. Marino-Enriquez A, Ou WB, Weldon CB, Fletcher JA, Perez-Atayde AR. ALK rearrangement in sickle cell trait-associated renal medullary carcinoma. Genes Chromosomes Cancer 2011;50:146–53.

Identification of a novel fusion, SQSTM1-ALK, in ALK-positive large B-cell lymphoma

Kengo Takeuchi,[1] Manabu Soda,[2] Yuki Togashi,[1] Yasunori Ota,[3] Yasunobu Sekiguchi,[4] Satoko Hatano,[1] Reimi Asaka,[1] Masaaki Noguchi,[4] and Hiroyuki Mano[2,5]

[1]Pathology Project for Molecular Targets, The Cancer Institute, Japanese Foundation for Cancer Research, Tokyo; [2]Division of Functional Genomics, Jichi Medical University, Tochigi; [3]Department of Pathology, Toranomon Hospital, Tokyo; [4]Department of Hematology, Urayasu Hospital, Juntendo University, Chiba; [5]CREST, Japan Science and Technology Agency, Saitama, Japan

ABSTRACT

ALK-positive large B-cell lymphoma is a rare subtype of lymphoma, and most cases follow an aggressive clinical course with a poor prognosis. We examined an ALK-positive large B-cell lymphoma case showing an anti-ALK immunohistochemistry pattern distinct from those of 2 known ALK fusions, CLTC-ALK and NPM-ALK, for the presence of a novel ALK fusion; this led to the identification of SQSTM1-ALK. SQSTM1 is an ubiquitin binding protein that is associated with oxidative stress, cell signaling, and autophagy. We showed transforming activities of SQSTM1-ALK with a focus formation assay and an *in vivo* tumorigenicity assay using 3T3 fibroblasts infected with a recombinant retrovirus encoding SQSTM1-ALK. ALK-inhibitor therapies are promising for treating ALK-positive large B-cell lymphoma, especially for refractory cases. SQSTM1-ALK may be a rare fusion, but our data provide novel biological insights and serve as a key for the accurate diagnosis of this rare lymphoma.

Key words: ALK-positive, large B-cell lymphoma, fusion.

Citation: Takeuchi K, Soda M, Togashi Y, Ota Y, Sekiguchi Y, Hatano S, Asaka R, Noguchi M, Mano H. Identification of a novel fusion, SQSTM1-ALK, in ALK-positive large B-cell lymphoma. Haematologica 2011;96(03):464-467. doi:10.3324/haematol.2010.033514

Introduction

Anaplastic lymphoma kinase-positive large B-cell lymphoma (ALK+LBCL) is a rare subtype of lymphoma that was first described in 1997.[1] Approximately 50 cases have been reported to date,[2] with most cases (60%) following an aggressive clinical course.[3] In well-characterized cases, 3 genes have been reported as a fusion partner of *ALK*: *clathrin* (*CLTC-ALK*),[4-6] *nucleophosmin* (*NPM-ALK*),[7-8] and *SEC31A* (*SEC31A-ALK*).[9] In this paper, we report a case of ALK+LBCL that harbored a novel ALK fusion partner, sequestosome1 (SQSTM1).

Design and Methods

Materials

Biopsied specimens were fixed in 20% neutralized formalin and embedded in paraffin for conventional histopathological examination. We extracted DNA and total RNA from the snap-frozen specimens and subsequently purified the samples. Written informed consent was obtained from the patient. The study was approved by the Institutional Review Board of the Japanese Foundation for Cancer Research.

Immunohistochemistry

Formalin-fixed, paraffin-embedded tissue was used. For antigen retrieval, we heated the slides for 40 min at 97°C in Target Retrieval Solution (pH 9.0; Dako), and subsequently detected the immune complexes with a dextran polymer reagent (EnVision+DAB system, Dako) and an AutoStainer instrument (Dako).

Isolation of ALK fusion cDNA

To obtain cDNA fragments corresponding to novel ALK fusion genes, we used an inverse reverse transcription-polymerase chain reaction (RT-PCR) method slightly modified from one previously reported.[10] Double-stranded cDNA was synthesized from 2 μg of total RNA with 1 pM of the primer ALKREVex22-23 (5′-TGGTTGAATTTGCTGATGATC-3′) and a cDNA Synthesis System (Roche), and was self-ligated by incubation overnight with T4 DNA ligase (TaKaRa Bio). We subjected the resulting circular cDNA to PCR (35 cycles of 94°C for 15 sec, 62°C for 30 sec, and 72°C for 1 min) with primers ALKREV3T (5′-CTGATGGAGGAGGTCTTGCC-3′) and ALKFWDex20-21 (5′-ATTCGGGGTCTGGGCCAT-3′) in a final volume of 20 μL. We subjected 1 μL of the 1:100 diluted reaction products to a second PCR step (the same settings as above), with primers ALKREV4T (5′-GGTTGTAGTCGGTCATGATGGTC-3′) and ALKFWDex21-22 (5′-AGTGGCTGTGAAGACGCTGC-3′) in a final volume of 20 μL. The resulting products were purified by gel extraction and directly sequenced in both directions with primers ALKFWDex20-21 and ALKREV4T.

The fusion point of *SQSTM1-ALK* cDNA was amplified by RT-

The online version of this article has a Supplementary Appendix.

Acknowledgments: we thank Drs. Masaru Hosone, Yuichi Sugisaki, Koji Izutsu, Shuji Momose, and Jun-ichi Tamaru for their advice. The nucleotide sequences of the cDNAs for SQSTM1-ALK have been deposited in the DDBJ/EMBL/GenBank databases under the accession number, AB583922. Manuscript received on September 12, 2010. Revised version arrived on November 11, 2010. Manuscript accepted on November 29, 2010.

Correspondence: Kengo Takeuchi, M.D., Ph.D. Pathology Project for Molecular Targets, Cancer Institute, Japanese Foundation for Cancer Research. 3-8-31 Ariake, Koto, Tokyo 135-8550, Japan. E-mail: kentakeuchi-tky@umin.net; Phone: international +81-3-3520-0111; Fax: international +81-3-3570-0558.

PCR with primers SQSTM1 565F (5′-AAACACGGACACTTCGGGT-3′) and ALK3078RR (5′-ATCCAGTTCGTCCTGTTCAGAGC-3′).

Full-length *SQSTM1-ALK* cDNA was obtained from the specimen by RT-PCR with primers SQSTM1v1-F90 (5′-CTCGCTATGGCGTCGCTCACCGTGAA-3′) and KA-W-cDNA-out-AS (5′-CCACGGTCTTAGGGATCCCAAGG-3′).

Fluorescence in situ hybridization (FISH)

We performed FISH analysis of the gene fusion for unstained slides (4 μm thick) with bacterial artificial chromosome (BAC) clone-derived DNA probes for *ALK* (RP11-984I21, RP11-62B19) and *SQSTM1* (RP11-55M16).

Transformation assay for ALK fusion protein

We analyzed the transforming activity of SQSTM1-ALK as described previously.[11-13] Briefly, cDNA for SQSTM1-ALK was inserted into the retroviral expression plasmid pMXS.[14] The resulting plasmid and similar pMXS-based expression plasmids for EML4-ALK variant 1 or NPM-ALK were used to generate recombinant ecotropic retroviruses, which were then used to infect mouse 3T3 fibroblasts. We evaluated formation of transformed foci after culturing the cells for 14 days. We subcutaneously injected the same set of 3T3 cells into nu/nu mice and examined tumor formation after 20 days.

PCR for IGH gene rearrangement

Genomic PCR was used for amplification of the rearranged *IGH* gene using the primers FR2A 5′-TGG(A/G)TCCG(A/C)CAG(C/G)C(C/T)(C/T)CNGG-3′ and LJH 5′-ACCTGAGGAGACGGTGACC-3′. Several clones were sequenced after subcloning the PCR product into pGEM-T-Easy Vector (Promega).

Results and Discussion

Case presentation

A 67-year old man was admitted with a tumor in the left side of his neck. A systemic workup revealed swelling of cervical, mediastinal, and hilar lymph nodes. Blood counts were within normal ranges. Lactose dehydrogenase was slightly elevated (223 IU/L) in peripheral blood with high IgG (2,425 mg/dL), normal IgA (157 mg/dL) and low IgM (32 mg/dL) levels.

Histopathological examination of the biopsied specimen from the cervical lymph node showed a diffuse infiltrate of tumor cells with a round, vesicular nucleus containing a centrally located large nucleolus. The cytoplasm was abundant (Figure 1A). These features may be consistent with immunoblasts or plasmablasts, but the size of tumor cells was large compared with typical immunoblasts and plasmablasts. Immunophenotypically, the tumor cells were negative for CD3, CD4, CD5, CD10, CD20, CD57, CD79a, and most cytokeratins (CK5/6, CK8, CK19, CK20); focally positive for CD30 and cytokeratins (AE1/AE3, CAM5.2, CK7, CK18) (Figure 1B); weakly pos-

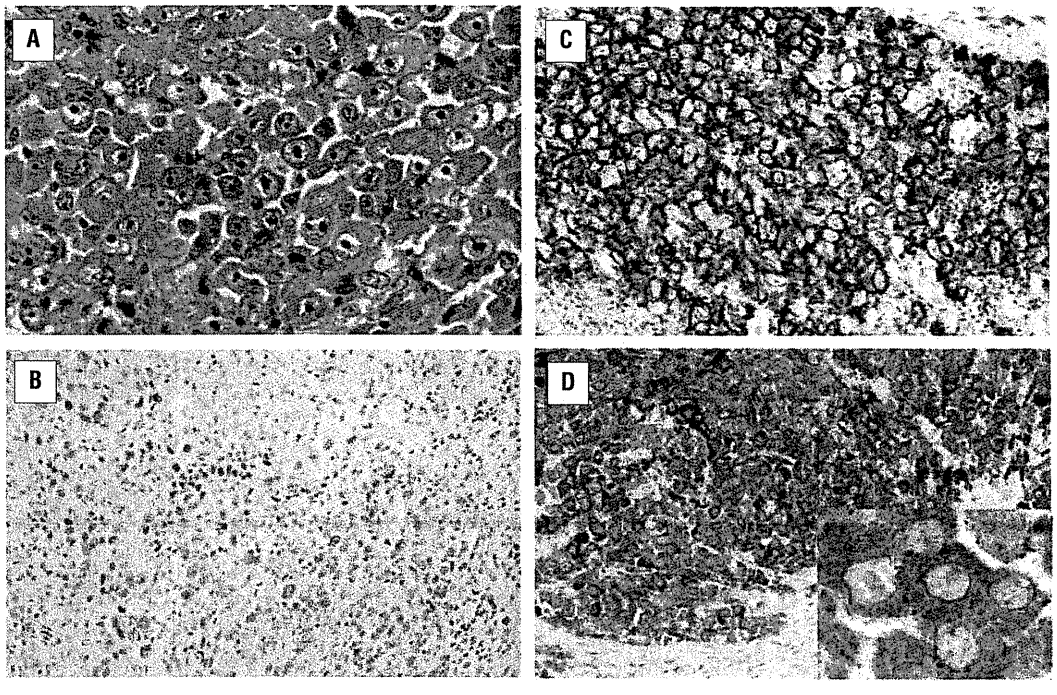

Figure 1. Histopathology of SQSTM1-ALK-positive large B-cell lymphoma. (A) The pattern of tumor infiltration was diffuse. The lymphoma cells were large with abundant cytoplasm and had round, vesicular nuclei, each containing a centrally located large nucleolus. These features may be consistent with immunoblasts or plasmablasts, but the size of tumor cells was extremely large compared with these typical cell types (Magnification 40×). (B) Some lymphoma cells expressed cytokeratin (AE1/AE3) (Magnification 20×). (C) Syndecan1/CD138 was strongly expressed (Magnification 20×). (D) In anti-ALK immunohistochemistry, a diffuse cytoplasmic staining pattern with ill-demarcated spots was clearly shown (Magnification 20×).

itive for PAX5; and positive for CD138 (Figure 1C), EMA, and ALK (Figure 1D). The positivity of focal cytokeratin, which has been reported in a small proportion of ALK+LBCL cases,[15] and the cytomorphology of this case may have led to a misdiagnosis of undifferentiated metastatic carcinoma. The presence of *ALK* translocation was demonstrated by an ALK split FISH assay, which was performed at a commercial laboratory (*data not shown*). The tumor cells were positive for PAX5, which is suggestive of ALK+LBCL. However, we carefully excluded a possibility of metastasis of ALK-positive lung cancer[10] because the tumor cells were positive for some cytokeratins and immunohistochemistry for immunoglobulins was not evaluable due to background staining. Immunohistochemistry for TTF1 was negative; this is usually positive in ALK-positive lung cancers.[16] In addition, PCR and sequencing analyses revealed that *IGH* was monoclonally rearranged and somatically hypermutated (*data not shown*).

The patient was diagnosed as having ALK+LBCL and achieved complete remission after 6 cycles of cyclophosphamide, doxorubicin, vincristine, and prednisone (CHOP) treatment. Four months later, however, he relapsed.

Identification of SQSTM1-ALK

The 2 major ALK fusions in ALK+LBCL are CLTC-ALK and NPM-ALK, and they show a coarse granular cytoplasmic pattern and a nuclear and cytoplasmic pattern in anti-ALK immunohistochemistry, respectively. In the present case, anti-ALK immunohistochemistry showed a diffuse cytoplasmic staining pattern with ill-demarcated spots (Figure 1D), which was different from either of the former 2 patterns. Therefore, we carried out inverse RT-PCR to examine the presence of a novel fusion of *ALK*. We indeed isolated a cDNA containing the exon 5 of *SQSTM1* in-frame fused to the exon 20 of *ALK* (Figure 2A). A separate RT-PCR assay amplified the fusion point of *SQSTM1-ALK* cDNA (*data not shown*). To confirm the chromosome rearrangement, we performed *SQSTM1-ALK* fusion FISH. This result was consistent with the presence of a t(2;5)(p23.1;q35.3) leading to the generation of *SQSTM1-ALK* (Figure 2B). The complete sequences of SQSTM1-ALK are shown in the *Online Supplementary Figure S1*.

SQSTM1 is an ubiquitin binding protein that is associated with oxidative stress, cell signaling, and autophagy.[17-20] Autophagosomal membrane protein LC3/Atg8 binds SQSTM1 and makes SQSTM1-containing protein aggregate to the autophagosome.[21] Mutations within *SQSTM1* are identified in patients with Paget's disease of bone.[22]

SQSTM1 is located very near *NPM*, which is on 5q35.1. Therefore, the cytogenetic findings of the NPM-ALK-positive and the SOSTM1-ALK-positive lymphomas may be similar, and this may mean that SQSTM1-ALK occurrence in lymphoma may be underestimated. As mentioned, however, NPM-ALK and SQSTM1-ALK differ in terms of the anti-ALK immunostaining pattern. NPM has a nuclear transport signal, while SQSTM1 does not. Therefore, NPM-ALK shows a nuclear and cytoplasmic staining pattern while SQSTM1-ALK shows only a cytoplasmic staining pattern. ALK is a representative "promiscuous" molecule because of its various fusion partners. The subcellular localization of ALK fusions depends on the fusion partners. The anti-ALK immunohistochemical staining pattern is, therefore, a simple and useful means to identify the possible partner in a tested case and, in fact, has prompted the identification of many ALK fusion partners, including the present case.

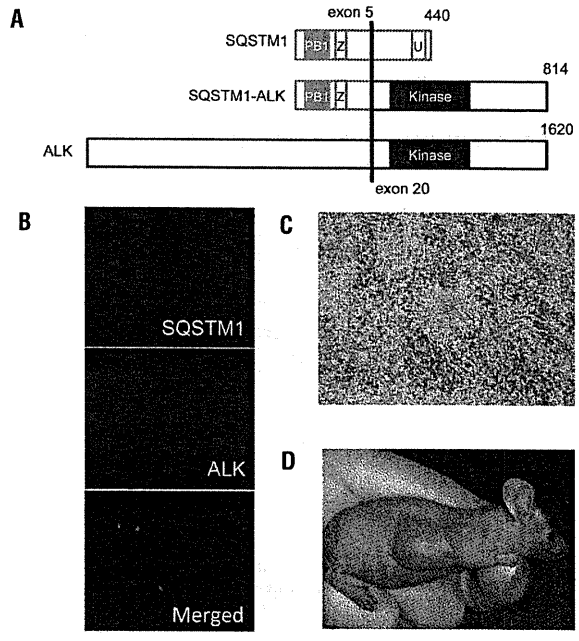

Figure 2. Discovery of *SQSTM-ALK* fusion gene. (A) A chromosome translocation, t(2;5)(p23.1;q35.3), generates a cDNA fusion in which exon 5 of *SQSTM* is joined to the *ALK* cDNA for the intracellular region of its encoded protein (containing the tyrosine kinase domain). Numbers indicate amino acid positions of each protein. PB1: Phox and Bem1p; Z: atypical zinc finger; U: ubiquitin-associated. (B) A section of the specimen for the present case was subjected to FISH with an *SQSTM1-ALK* fusion assay. Nuclei are stained blue with DAPI. (C) Murine 3T3 fibroblasts were infected with retroviruses expressing SQSTM1-ALK. The cells were photographed after culture for 14 days. (D) A nude mouse was injected subcutaneously with 3T3 cells infected as in (C), and tumor formation was examined after 20 days.

Transforming activities of SQSTM1-ALK

We generated a recombinant retrovirus encoding SQSTM1-ALK and used it to infect cultured 3T3 fibroblasts. Infection with the virus, but not with an empty virus, resulted in the formation of multiple transformed foci *in vitro* (Figure 2C). As control experiments for formation, EML4-ALK (variant 1) and NPM-ALK similarly produced transformed foci (*data not shown*). The same 3T3 cells were injected into nude mice for an *in vivo* tumorigenicity assay. As expected, 3T3 cells expressing SQSTM1-ALK developed subcutaneous tumors at all injection sites within an observation period of 20 days (Figure 2D), confirming the transforming potential of the novel fusion kinase, SQSTM1-ALK.

All ALK fusion partners identified so far except NPM and moesin (MSN) have a coiled-coil domain(s) in their sequences, and the domain is conserved in its fusion form. The coiled-coil domain allows the protein to homodimerize. The tyrosine kinase domain of the ALK fusions is constitutively phosphorylated and activated through homodimerization via the coiled-coil domain. It has been specu-

lated that the binding properties of MSN to cell membrane proteins lead to the dimerization of MSN-ALK proteins, enabling the constitutive phosphorylation of the chimeric MSN-ALK protein.[23] SQSTM1 does not harbor a coiled-coil domain and does not bind to membrane proteins. Instead, it has the Phox and Bem1p (PB1) domain in its N-terminus and forms heteromeric and homomeric complexes mediated by this domain.[24] Therefore, SQSTM1-ALK probably homodimerizes through the PB1 domain, leading to constitutive activation of the ALK kinase domain.

In conclusion, we reported a novel ALK fusion, SQSTM1-ALK, and its oncogenicity. ALK+LBCL is an aggressive lymphoma with poor prognosis;[3] ALK inhibitors are promising therapeutic agents for this condition. SQSTM1-ALK may be a rare fusion, but our data provide novel biological insights and may serve as a key to the accurate diagnosis of this rare lymphoma.

Authorship and Disclosures

The information provided by the authors about contributions from persons listed as authors and in acknowledgments is available with the full text of this paper at www.haematologica.org.

Financial and other disclosures provided by the authors using the ICMJE (www.icmje.org) Uniform Format for Disclosure of Competing Interests are also available at www.haematologica.org.

References

1. Delsol G, Lamant L, Mariame B, Pulford K, Dastugue N, Brousset P, et al. A new subtype of large B-cell lymphoma expressing the ALK kinase and lacking the 2; 5 translocation. Blood. 1997;89(5):1483-90.
2. Beltran B, Castillo J, Salas R, Quinones P, Morales D, Hurtado F, et al. ALK-positive diffuse large B-cell lymphoma: report of four cases and review of the literature. J Hematol Oncol. 2009;2:11.
3. Laurent C, Do C, Gascoyne RD, Lamant L, Ysebaert L, Laurent G, et al. Anaplastic lymphoma kinase-positive diffuse large B-cell lymphoma: a rare clinicopathologic entity with poor prognosis. J Clin Oncol. 2009;27(25):4211-6.
4. Gascoyne RD, Lamant L, Martin-Subero JI, Lestou VS, Harris NL, Muller-Hermelink HK, et al. ALK-positive diffuse large B-cell lymphoma is associated with Clathrin-ALK rearrangements: report of 6 cases. Blood. 2003;102(7):2568-73.
5. De Paepe P, Baens M, van Krieken H, Verhasselt B, Stul M, Simons A, et al. ALK activation by the CLTC-ALK fusion is a recurrent event in large B-cell lymphoma. Blood. 2003;102(7):2638-41.
6. Chikatsu N, Kojima H, Suzukawa K, Shinagawa A, Nagasawa T, Ozawa H, et al. ALK+, CD30-, CD20- large B-cell lymphoma containing anaplastic lymphoma kinase (ALK) fused to clathrin heavy chain gene (CLTC). Mod Pathol. 2003;16(8):828-32.
7. Onciu M, Behm FG, Downing JR, Shurtleff SA, Raimondi SC, Ma Z, et al. ALK-positive plasmablastic B-cell lymphoma with expression of the NPM-ALK fusion transcript: report of 2 cases. Blood. 2003;102(7):2642-4.
8. Adam P, Katzenberger T, Seeberger H, Gattenlohner S, Wolf J, Steinlein C, et al. A case of a diffuse large B-cell lymphoma of plasmablastic type associated with the t(2;5)(p23;q35) chromosome translocation. Am J Surg Pathol. 2003;27(11):1473-6.
9. Van Roosbroeck K, Cools J, Dierickx D, Thomas J, Vandenberghe P, Stul M, et al. ALK-positive large B-cell lymphomas with cryptic SEC31A-ALK and NPM1-ALK fusions. Haematologica. 2010;95(3):509-13.
10. Takeuchi K, Choi YL, Togashi Y, Soda M, Hatano S, Inamura K, et al. KIF5B-ALK, a novel fusion oncokinase identified by an immunohistochemistry-based diagnostic system for ALK-positive lung cancer. Clin Cancer Res. 2009;15(9):3143-9.
11. Soda M, Choi YL, Enomoto M, Takada S, Yamashita Y, Ishikawa S, et al. Identification of the transforming EML4-ALK fusion gene in non-small-cell lung cancer. Nature. 2007;448(7153):561-6.
12. Takeuchi K, Choi YL, Soda M, Inamura K, Togashi Y, Hatano S, et al. Multiplex reverse transcription-PCR screening for EML4-ALK fusion transcripts. Clin Cancer Res. 2008;14(20):6618-24.
13. Choi YL, Takeuchi K, Soda M, Inamura K, Togashi Y, Hatano S, et al. Identification of novel isoforms of the EML4-ALK transforming gene in non-small cell lung cancer. Cancer Res. 2008;68(13):4971-6.
14. Onishi M, Kinoshita S, Morikawa Y, Shibuya A, Phillips J, Lanier LL, et al. Applications of retrovirus-mediated expression cloning. Exp Hematol. 1996;24:324-9.
15. Reichard KK, McKenna RW, Kroft SH. ALK-positive diffuse large B-cell lymphoma: report of four cases and review of the literature. Mod Pathol. 2007;20(3):310-9.
16. Inamura K, Takeuchi K, Togashi Y, Hatano S, Ninomiya H, Motoi N, et al. EML4-ALK lung cancers are characterized by rare other mutations, a TTF-1 cell lineage, an acinar histology, and young onset. Mod Pathol. 2009;22(4):508-15.
17. Komatsu M, Kurokawa H, Waguri S, Taguchi K, Kobayashi A, Ichimura Y, et al. The selective autophagy substrate p62 activates the stress responsive transcription factor Nrf2 through inactivation of Keap1. Nat Cell Biol. 2010;12(3):213-23.
18. Kirkin V, McEwan DG, Novak I, Dikic I. A role for ubiquitin in selective autophagy. Mol Cell. 2009;34(3):259-69.
19. Seibenhener ML, Geetha T, Wooten MW. Sequestosome 1/p62--more than just a scaffold. FEBS Lett. 2007;581(2):175-9.
20. Bjorkoy G, Lamark T, Johansen T. p62/SQSTM1: a missing link between protein aggregates and the autophagy machinery. Autophagy. 2006;2(2):138-9.
21. Pankiv S, Clausen TH, Lamark T, Brech A, Bruun JA, Outzen H, et al. p62/SQSTM1 binds directly to Atg8/LC3 to facilitate degradation of ubiquitinated protein aggregates by autophagy. J Biol Chem. 2007;282(33):24131-45.
22. Laurin N, Brown JP, Morissette J, Raymond V. Recurrent mutation of the gene encoding sequestosome 1 (SQSTM1/p62) in Paget disease of bone. Am J Hum Genet. 2002;70(6):1582-8.
23. Tort F, Pinyol M, Pulford K, Roncador G, Hernandez L, Nayach I, et al. Molecular characterization of a new ALK translocation involving moesin (MSN-ALK) in anaplastic large cell lymphoma. Lab Invest. 2001;81(3):419-26.
24. Lamark T, Perander M, Outzen H, Kristiansen K, Overvatn A, Michaelsen E, et al. Interaction codes within the family of mammalian Phox and Bem1p domain-containing proteins. J Biol Chem. 2003;278(36):34568-81.

Molecular Cell
Article

MCPIP1 Ribonuclease Antagonizes Dicer and Terminates MicroRNA Biogenesis through Precursor MicroRNA Degradation

Hiroshi I. Suzuki,[1] Mayu Arase,[1] Hironori Matsuyama,[1] Young Lim Choi,[2] Toshihide Ueno,[3] Hiroyuki Mano,[2,3] Koichi Sugimoto,[4] and Kohei Miyazono[1,*]
[1]Department of Molecular Pathology
[2]Department of Medical Genomics
Graduate School of Medicine, University of Tokyo, 7-3-1 Hongo, Bunkyo-ku, Tokyo 113-0033, Japan
[3]Division of Functional Genomics, Jichi Medical University, 3311-1 Yakushiji, Shimotsukeshi, Tochigi 329-0498, Japan
[4]Division of Hematology, Department of Internal Medicine, Juntendo University School of Medicine, 2-1-1 Hongo, Bunkyo-ku, Tokyo 113-8421, Japan
*Correspondence: miyazono@m.u-tokyo.ac.jp
DOI 10.1016/j.molcel.2011.09.012

SUMMARY

MicroRNAs (miRNAs) are versatile regulators of gene expression and undergo complex maturation processes. However, the mechanism(s) stabilizing or reducing these small RNAs remains poorly understood. Here we identify mammalian immune regulator MCPIP1 (Zc3h12a) ribonuclease as a broad suppressor of miRNA activity and biogenesis, which counteracts Dicer, a central ribonuclease in miRNA processing. MCPIP1 suppresses miRNA biosynthesis via cleavage of the terminal loops of precursor miRNAs (pre-miRNAs). MCPIP1 also carries a vertebrate-specific oligomerization domain important for pre-miRNA recognition, indicating its recent evolution. Furthermore, we observed potential antagonism between MCPIP1 and Dicer function in human cancer and found a regulatory role of MCPIP1 in the signaling axis comprising miR-155 and its target c-Maf. These results collectively suggest that the balance between processing and destroying ribonucleases modulates miRNA biogenesis and potentially affects pathological miRNA dysregulation. The presence of this abortive processing machinery and diversity of MCPIP1-related genes may imply a dynamic evolutional transition of the RNA silencing system.

INTRODUCTION

miRNAs constitute a large family of short endogenous, noncoding RNA molecules that regulate posttranscriptional gene silencing. miRNAs operate in many important aspects of diverse biological programs, including differentiation, proliferation, and cell death, and their deregulation is associated with an expanding number of disease processes such as cancer and cardiovascular diseases. The canonical miRNA biogenesis pathway is composed of several steps in mammalian cells (Davis and Hata, 2009; Siomi and Siomi, 2010). The primary transcripts of miRNA genes, primary miRNAs (pri-miRNAs), are transcribed and endonucleolytically cleaved to precursor miRNAs (pre-miRNAs) by the nuclear RNase III Drosha. The pre-miRNAs are exported into the cytoplasm by exportin-5 (XPO5) and further cleaved to a double-stranded miRNA duplex by another RNaseIII, Dicer. The mature miRNA strand is subsequently incorporated into the RNA-induced silencing complex (RISC). While it has been recently shown that multiple steps of miRNA biogenesis are regulated by several RNA binding factors such as Lin-28, hnRNP A1, and KSRP, and crosstalk with intracellular signaling networks (Suzuki and Miyazono, 2011; Suzuki et al., 2009), *cis*-regulatory elements and *trans*-acting factors responsible for stabilization or reduction of miRNAs have been largely unknown.

In mammalian systems, previous studies have established the close relationship between the immune system and the small RNA regulation. miRNA expression is dynamically regulated during the immune response (Moschos et al., 2007; O'Connell et al., 2010), and miRNA biogenesis also seems actively regulated in this setting; KSRP has been shown to regulate miRNA maturation in macrophage activation (Ruggiero et al., 2009).

In the present study, we identify the mammalian immune regulator, MCPIP1 (monocyte chemoattractant protein [MCP]-1-induced protein 1, also known as Zc3h12a [Zinc-finger CCCH-type containing 12A]), as a broad suppressor of the miRNA pathway. MCPIP1 with NYN nuclease domain preferentially cleaves the terminal loops of pre-miRNAs and counteracts Dicer, leading to the inhibition of de novo miRNA synthesis. Inverse correlation between MCPIP1 and Dicer function was seen in human lung cancer, in which low Dicer expression is associated with poor prognosis. These results suggest that the balance of productive and abortive ribonucleases modulates miRNA biogenesis and potentially affects pathological miRNA dysregulation. The presence of this abortive processing machinery and diversity of MCPIP1-related genes also implies a dynamic evolutional transition of the RNA silencing system.

RESULTS

Silencing of miRNA Activity by a CCCH Zinc-Finger Protein, MCPIP1

We screened regulator(s) of the miRNA pathway employing luciferase reporter constructs with the complementary sequence to several miRNAs in the 3′ UTR. Based on a close relationship between small RNA and immune system (O'Connell et al., 2010), we particularly focused on the immune response-associated genes harboring a potential RNA binding domain. In this process, we found that, although the ectopic expression of short fragments of pri-miRNAs caused a 5- to 10-fold reduction of luciferase activity in this assay, human MCPIP1 (also known as Zc3h12a), one of the CCCH-type zinc-finger proteins with RNA-binding potential (Liang et al., 2008a), remarkably attenuated the RNAi activity mediated by introduction of pri-miR-122 (Figure 1A). We also confirmed similar results using various mammalian cell lines such as HeLa, HepG2, and Cos-7 cells to exclude the possibility of cell-type-specific phenomena.

miRNA silencing activity of MCPIP1 was extended to other miRNAs, such as miR-21 and miR-135b (Figures 1B and 1C) and recapitulated in the experiments using miR-135b and its target, *adenomatous polyposis coli* (*APC*) 3′ UTR (Figure 1D) (Nagel et al., 2008). In addition, siRNA-mediated MCPIP1 knockdown consistently enhanced endogenous miRNA activity (Figure 1E) in HepG2 hepatocellular carcinoma cells, which express MCPIP1 at the basal level. These results suggested that MCPIP1 suppresses miRNA functions in gene silencing.

Inhibition of miRNA Biogenesis by MCPIP1

About 60 CCCH-type zinc-finger proteins have been identified so far in mouse and human (Liang et al., 2008a). MCPIP1 exerts the most potent suppressive activity to miRNAs among the MCPIP family (MCPIP1/2/3/4) and other tested CCCH-type zinc-finger proteins such as Cpsf4, Cpsf4l, Zfp36, Rc3h1, and Rc3h2 (Figure 1A), which prompted us to focus on the MCPIP1 function.

Because some CCCH proteins, including Zfp36 and Rc3h1, are involved in RNA metabolism (Liang et al., 2008a) and MCPIP1 appears to have an influence on broad miRNA activities, we examined a potential impact of MCPIP1 on the intracellular fates of miRNAs and their precursors. Quantitative RT-PCR analysis showed that MCPIP1 remarkably suppressed mature miRNA production from ectopically expressed pri-miRNAs of various miRNAs, such as miR-135b, -146a, -21, -155, -143, and -145 (Figures 1F, 1G, and S1A–S1D). Interestingly, MCPIP1 decreased the expression levels of precursor forms (pre-miRNAs) of these miRNAs, but the pri-miRNAs showed no significant change (Figures 1F, 1G, and S1A–S1D). Northern blot analyses confirmed these observations (Figures 1H, 1I, and S1E–S1H). MCPIP1 overexpression also decreased the mature miRNA levels of endogenously expressed miRNAs by 20%–30%.

Two major steps of mammalian miRNA biogenesis are executed by nuclear Drosha and cytoplasmic Dicer. We then asked in which cellular compartment MCPIP1 localizes and functions. Immunocytochemical analysis showed that MCPIP1 localized mainly in the cytoplasm as dot-like structures (Figure 2A). GFP-tagged MCPIP1 also partly colocalized with HA-tagged GW182 or Dcp1a, suggesting that MCPIP1 localizes in GW bodies or P bodies (Figure 2B). Colocalization frequency of GFP-MCPIP1 with HA-GW182 was higher than that with HA-Dcp1a, while GFP-MCPIP1 was often adjacent to Dcp1a-positive foci. In addition, MCPIP1 strongly reduced miRNA expression and activity under pri-miRNA overexpression (Figure 1), but showed no significant effect on miRNA activity upon miRNA duplex introduction (Figures 2C and 2D) or the stability of introduced miRNA duplexes (Figures 2E and 2F).

Next, we confirmed that MCPIP1 knockdown elevated the intrinsic levels of several mature miRNAs, such as miR-21, -26a, -107, -182, -146a, -17-5p, and -135b in HepG2 cells, without concomitant changes of the corresponding pri-miRNAs (Figure 2G) and enhanced the miRNA maturation efficacy from ectopically expressed pri-miRNAs (Figures S2A–S2D). Microarray analysis of miRNA expression profile demonstrated that wide proportion of miRNAs tended to be upregulated by MCPIP1 suppression (Figure 2H). These results thus proposed that MCPIP1 acts on pre-miRNAs in the cytoplasm to inhibit de novo maturation of a broad range of miRNA species, without deteriorating the major molecular components of the miRNA pathway (Figure S2E). Immunoblot analysis also confirmed endogenous expression of Dicer and MCPIP1 in the cell lines used in this study (Figure S2F).

Cleavage of Pre-miRNAs by MCPIP1 Ribonuclease

The N terminus of MCPIP1 (residues 133–300) is well conserved among other related proteins including MCPIP2, MCPIP3, and MCPIP4 and has been previously referred to as *N*edd4-BP1, bacterial *Yac*P *N*uclease (NYN) domain (Anantharaman and Aravind, 2006) (Figures 3A and S3A). The NYN domain shares a similar protein fold with two characterized nuclease domains, the PilT N-terminal (PIN) domain and FLAP nuclease domain, and is thus predicted to exert nuclease activity (Figures 3A and S3A–S3B) (Anantharaman and Aravind, 2006). In fact, it has been recently shown that MCPIP1/Zc3h12a is involved in mRNA decay of several genes as a ribonuclease (Matsushita et al., 2009).

We therefore examined whether pre-miRNAs can be cleaved by MCPIP1 through in vitro cleavage assay using the radiolabeled pre-miRNAs and FLAG-tagged MCPIP1. When the radiolabeled pre-miRNAs were incubated with immunoprecipitated FLAG-tagged MCPIP1 in vitro, the resultant products migrated as a broad and fuzzy band around 25–35 nt in length on electrophoresis, while FLAG-Dicer generated ~22 nt mature miRNA duplex (Figures 3B and 3C), demonstrating that MCPIP1 targets pre-miRNAs as a ribonuclease. We observed that both Dicer and MCPIP1 cleaved pre-miRNAs in a time- and dose-dependent manner (Figures S3C and S3D). The NYN domain of MCPIP1 has the canonical four conserved acidic residues (Asp 141, Asp 195, Asp 226, Asp 244) by analogy with other PIN domain RNases (Figure S3A) (Anantharaman and Aravind, 2006). These acidic residues have been reported to be crucial for metal ion binding and nuclease activity (Figure S3B). In accordance with these findings, mutant MCPIP1 with D141N mutation in the NYN domain, but not C306R mutation in the CCCH motif, failed to cleave pre-miRNAs in vitro (Figure 3D),

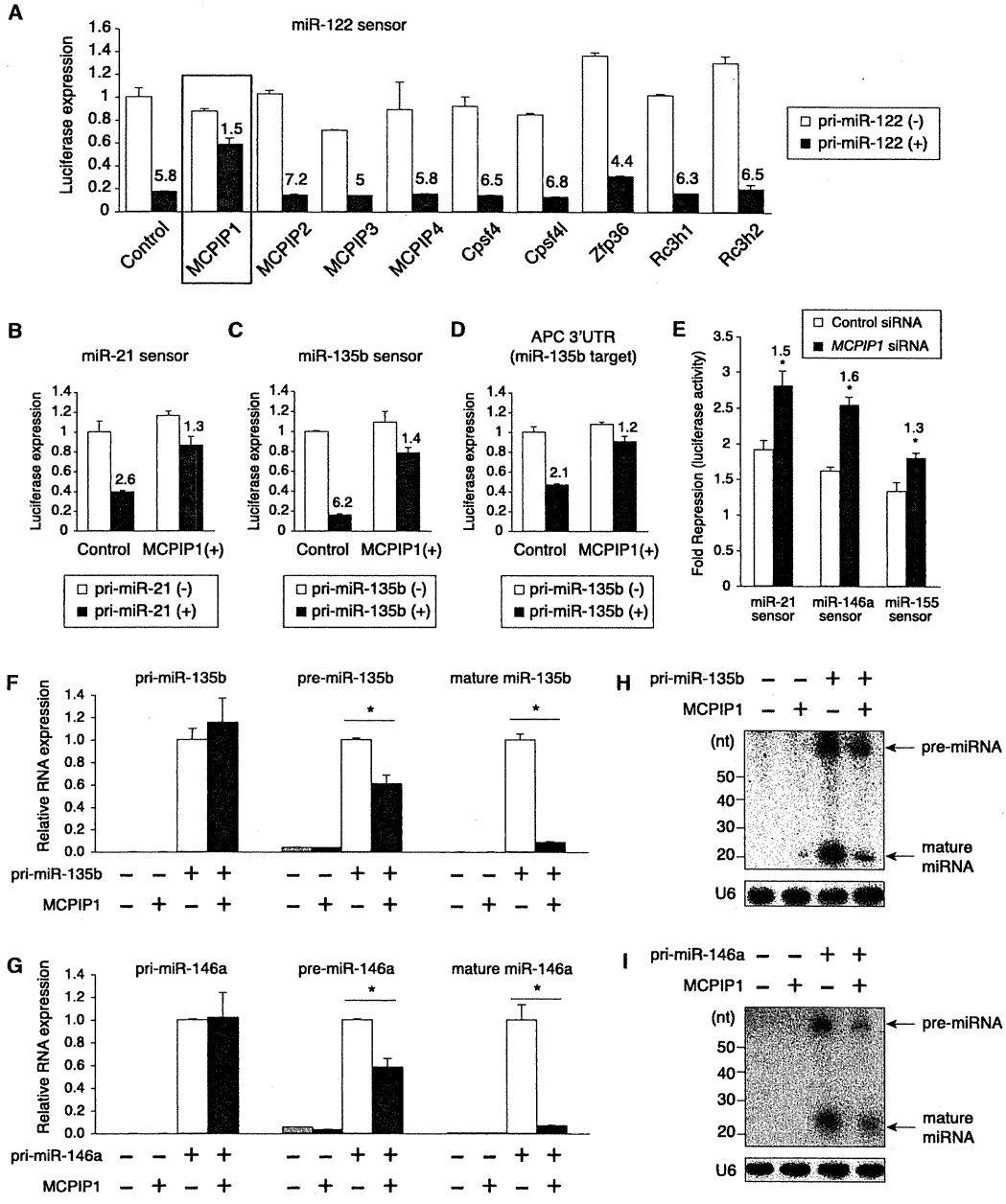

Figure 1. Suppression of miRNA Activity and Biogenesis by a CCCH-Type Zinc-Finger Gene, MCPIP1

(A) Effects of CCCH zinc-finger genes on miRNA activity. HEK293T cells were cotransfected with miR-122 sensor vector, pri-miR-122 expression vector, and the expression vectors of indicated genes, and applied to luciferase reporter assay at 48 hr after transfection. Numbers indicate the ratio of fold repression.

(B–D) Suppression of a range of miRNA activities by MCPIP1. miR-21 sensor (B), miR-135b sensor (C), or APC 3′ UTR luciferase vector (D), and the corresponding pri-miRNA expression vectors were ectopically expressed with/without MCPIP1 plasmids in HEK293T cells and subjected to luciferase reporter assay as shown in (A). Numbers indicate the ratio of fold repression.

(E) Enhancement of endogenous miRNA activity by MCPIP1 knockdown. HepG2 cells were transfected with indicated miRNA sensor vector and control siRNA or siRNA for *MCPIP1*. miRNA activities were measured by the ratio of the luciferase expression of miRNA sensor vector to that of control sensor vector (*$p < 0.05$, compared to Control siRNA; n = 3). Numbers indicate the ratio between control siRNA and *MCPIP1* siRNA.

(F–I) Inhibition of de novo miRNA biosynthesis by MCPIP1 overexpression. Quantitative RT-PCR (qRT-PCR) (F and G) and northern blot (H and I) analyses of RNA samples from HEK293T cells transfected with pri-miR-135b (F and H), -146a (G, I), and MCPIP1 (*$p < 0.05$, compared to empty vector; n = 3). See also Figure S1. Error bars represent SEM.

indicating the indispensable role of NYN domain for MCPIP1 ribonuclease function. Recombinant MCPIP1 proteins furthermore cleaved pre-miRNAs in a NYN domain-dependent manner in vitro (Figure 3E). On the other hand, a mutation in the CCCH motif (C306R), which had no significant effect on in vitro cleavage activity (Figures 3D and 3E), attenuated the miRNA suppressor activity of MCPIP1 in vivo (Figures 3F and 3G). This result suggests that the CCCH motif is additionally important for the in vivo function of MCPIP1, as investigated in Figure 7 (see below).

Functional Antagonism between MCPIP1 Ribonuclease and Dicer and Its Implication in Human Cancer

We then investigated whether MCPIP1 and its ribonuclease function can compete with Dicer function by in vitro competition analysis. As shown in Figures 4A and 4B, MCPIP1 antagonized Dicer-mediated pre-miRNA processing in vitro, depending on the intact NYN domain but not the CCCH motif, in a dose-dependent manner. Sequential in vitro cleavage analysis showed that MCPIP1-cleaved fragments were inefficient substrates for Dicer processing (Figure S4A). These results thus suggested that MCPIP1-mediated pre-miRNA cleavage could interfere with Dicer activity. In addition, absence of the degraded products in northern blot analyses suggested that MCPIP1-cleaved fragments may be unstable and subjected to a rapid subsequent degradation in vivo (Figure 1G, 1I, and S1E–S1H).

While individual miRNAs can behave as tumor suppressors or oncogenes (Suzuki and Miyazono, 2010), global miRNA downregulation has been shown to be a general trait of human cancers in several reports (Kumar et al., 2007; Lu et al., 2005; Ozen et al., 2008). Several mechanisms including downregulation of miRNA processing factors, such as Dicer and Drosha, and mutations of TRBP and XPO5 have been reported (Karube et al., 2005; Martello et al., 2010; Melo et al., 2010). Recent reports also revealed that certain oncogenesis-related molecules, such as p53, Smad, and estrogen receptor, are coupled with miRNA biogenesis (Suzuki and Miyazono, 2011). As evidence demonstrating the clinical relevance of these phenomena, reduced expression of Dicer is associated with poor survival in lung, ovarian, and breast cancer patients (Karube et al., 2005; Martello et al., 2010; Merritt et al., 2008).

Based on these observations, we investigated potential functional crosstalk between MCPIP1 and Dicer using several public gene expression datasets containing molecular and associated clinical details. We extracted gene sets associated negatively or positively with Dicer expression status ("Dicer High/Low Downregulated or Upregulated genes") from several human cancer cohorts, and performed gene set enrichment analysis (GSEA) (Subramanian et al., 2005) to examine whether these gene sets are overexpressed or underexpressed along the expression status of MCPIP1. During these trials, we found a potential antagonistic relationship between MCPIP1 and Dicer in human lung cancer. In the dataset of lung adenocarcinoma patients (Bild et al., 2006), GSEA demonstrated that "Dicer High/Low Downregulated genes" and "Dicer High/Low Upregulated genes" are enriched in patients with high MCPIP1 expression ("MCPIP1 High Case") and low MCPIP1 expression ("MCPIP1 Low Case"), respectively (Figure 4C). GSEA using the sets of potential miRNA target genes also demonstrated that a large proportion of miRNA target gene sets are upregulated in the MCPIP1-High group against the MCPIP1-Low group, while the opposite phenomenon was seen in the comparison between Dicer-High and -Low group (Figure 4D). Furthermore, we observed that high MCPIP1 levels are associated with poor survival in lung adenocarcinoma patients (Figure 4E), in an opposite manner to the association between low Dicer levels and poor prognosis (Karube et al., 2005; Merritt et al., 2008). Similar results were also obtained in another dataset of lung adenocarcinoma patients (Shedden et al., 2008) and a dataset of lung squamous cell carcinoma patients (Larsen et al., 2007) (Figures S4B–S4E). Together with in vitro antagonism, these findings demonstrate an inverse correlation between MCPIP1 expression and Dicer function in human cancer and suggest that MCPIP1 could drive opposite effects against Dicer on the transcriptome.

Modulation of miR-155/c-Maf axis by MCPIP1

We next investigated the impact of MCPIP1 on the function of endogenous miRNAs. MCPIP1 expression dynamically changes during the inflammatory response (Liang et al., 2008a; Liang et al., 2008b; Matsushita et al., 2009), and the importance of MCPIP1 in the immune system has recently emerged from a manifestation of profound autoimmune phenotype in mice lacking MCPIP1 (Matsushita et al., 2009). MCPIP1 has been shown to promote the mRNA decay of several inflammatory genes such as IL-6 as an endoRNase (Matsushita et al., 2009). The severity of autoimmune phenotype in *MCPIP1*$^{-/-}$ mice suggests the existence of additional targets of MCPIP1 other than IL-6 (Matsushita et al., 2009), and it might thus be partly explained by miRNA deregulation. In support of this notion, it has been shown that transgenic mice overexpressing several miRNAs, such as miR-17-92 and miR-155, exhibit autoimmune and/or lymphoproliferative diseases (Costinean et al., 2009; Xiao et al., 2008). Interestingly, increased and decreased expression of Th2 cytokine, IL-4, has been observed in miR-155$^{-/-}$ and *MCPIP1*$^{-/-}$ T cells, respectively (Matsushita et al., 2009; Rodriguez et al., 2007).

We then examined the potential involvement of MCPIP1 in regulation of miR-155 function in Jurkat T cells. In accordance with our previous results, MCPIP1 knockdown, in fact, caused miR-155 upregulation in Jurkat T cells (Figure 5A). MCPIP1 knockdown further suppressed the expression of the miR-155 target c-Maf and the induction of its transcriptional target IL-4 by phorbol myristate acetate (PMA) and ionomycin in a miR-155-dependent fashion (Rodriguez et al., 2007) (Figures 5B–5D), while IL-6 showed no significant effect on this axis (Figure S5A). These results are consistent with increased and decreased expression of IL-4 in miR-155$^{-/-}$ and *MCPIP1*$^{-/-}$ T cells (Matsushita et al., 2009; Rodriguez et al., 2007), reinforcing the physiological relevance of MCPIP1-mediated miRNA regulation. In addition, we observed that MCPIP1 is induced by lipopolysaccharide (LPS) and involved in the restriction of miR-155 upregulation under innate immune response and miR-16 downregulation during macrophage differentiation, while Dicer expression is not affected by LPS (Li et al., 2010) (Figures 5E, S5B, and S5C). These findings underscore active MCPIP1 involvement in miRNA biogenesis, together with the inverse

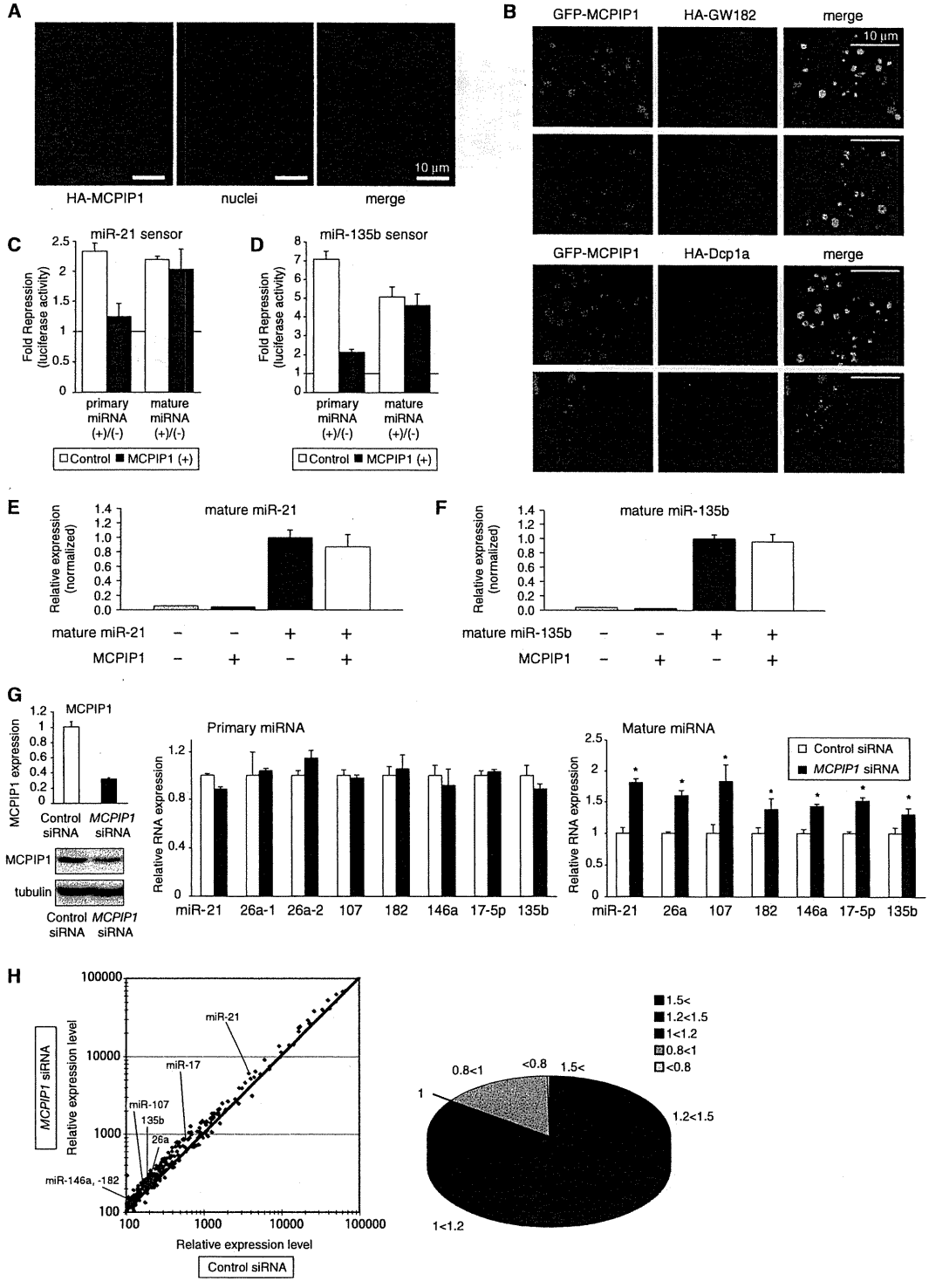

Figure 2. Cytoplasmic Localization of MCPIP1 and Enhancement of miRNA Maturation by MCPIP1 Depletion

(A) Immunocytochemical analysis of overexpressed HA-MCPIP1. Scale bar: 10 μm.

(B) Localization of GFP-MCPIP1, HA-GW182 and HA-Dcp1a.

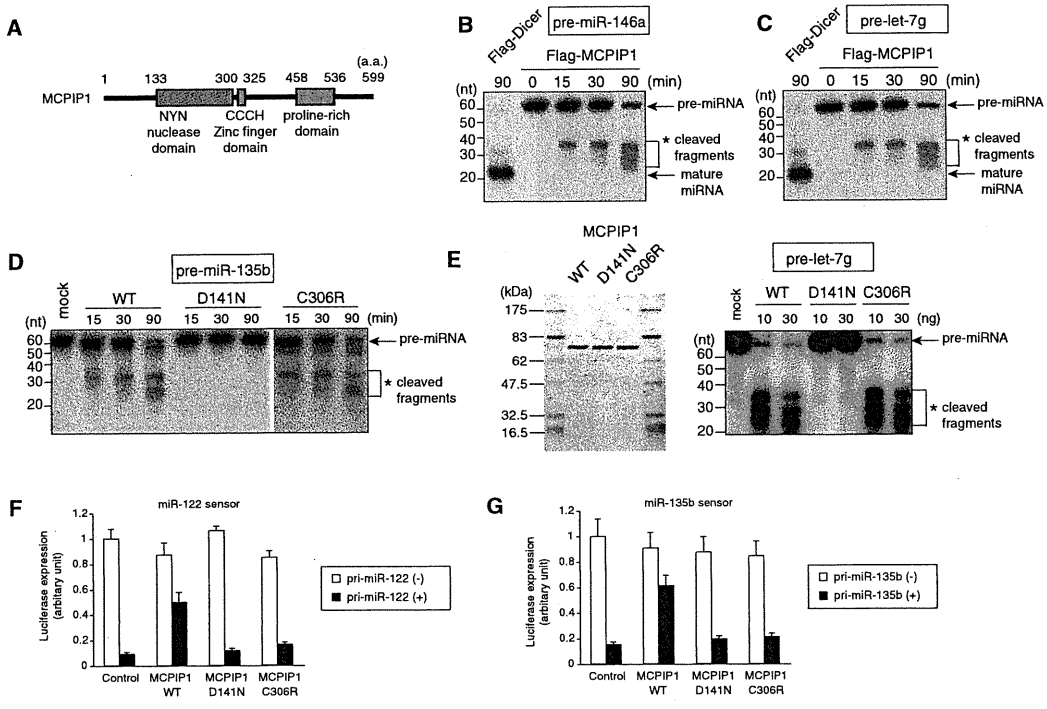

Figure 3. Cleavage of Pre-miRNAs by MCPIP1 Ribonuclease

(A) Domain organization of MCPIP1. NYN, *N*edd4-BP1, bacterial *Yac*P *N*uclease domain; CCCH, CCCH zinc-finger domain; PRD, proline-rich domain. See also Figure S3.

(B and C) In vitro cleavage of pre-miRNAs by MCPIP1. Radiolabeled pre-miR-146a (B) or pre-let-7g (C) were incubated with immunoprecipitated FLAG-Dicer or FLAG-MCPIP1 from HEK293T cells for indicated periods. The RNA was then extracted and analyzed by denaturing PAGE and autoradiography. 'nt' denotes nucleotides.

(D and E) Requirement of an intact NYN domain for in vitro RNase activity of MCPIP1. Radiolabeled pre-miRNAs were incubated with immunoprecipitated FLAG-MCPIP1 proteins (wild-type [WT], D141N, and C306R) (D) or recombinant MCPIP1 proteins (E).

(F and G) Effects of mutations in the NYN domain and CCCH domain on in vivo miRNA silencing activities. miR-122 sensor (F) or miR-135b sensor (G) and the corresponding pri-miRNA were coexpressed with/without MCPIP1 into HEK293T cells, and subjected to luciferase reporter assay (n = 3). Error bars represent SEM.

correlation between MCPIP1 and Dicer function in human cancer (Figure 4).

Targeting of the Terminal Loops of Pre-miRNAs by MCPIP1 Ribonuclease

The results shown in Figures 3 and 4 demonstrate that MCPIP1 cleaves pre-miRNAs and antagonizes Dicer function. We further analyzed the mode of MCPIP1 action on pre-miRNAs by direct cloning of pre-miRNA fragments cleaved by MCPIP1. Various 5′ and 3′ miRNA strands accompanied with additional bases from the terminal loop were recovered as the cleaved fragments of pre-miR-146a, pre-let-7g, pre-miR-135b, pre-miR-143 and pre-miR-16-1 (Figures 6A, 6B, and S6A–S6C), indicating that the primary cleavage sites of MCPIP1 were dispersed in the terminal loop of pre-miRNAs. A comparison with the predicted secondary structures of pre-miRNAs (Zuker, 2003) shows that MCPIP1 preferentially cleaves the unpaired regions around the terminal loops as an endoribonuclease (Figure 6C). Furthermore, addition of Lin-28b, an RNA-binding protein interacting with the terminal-loop of pre-let-7 (Heo et al., 2008), abolished the

(C and D) Differential effects of MCPIP1 on miRNA activities under introduction of pri-miRNAs and miRNA duplexes. miRNA sensor vectors (C: miR-21, D: miR-135b) and the corresponding pri-miRNA expression vectors or synthetic miRNA duplexes were cotransfected with/without MCPIP1 plasmids into HEK293T cells, and applied to luciferase reporter assay.

(E and F) Effect of MCPIP1 on the stability of introduced miRNAs duplexes. MCPIP1 plasmid was cotransfected with synthetic miRNA duplexes (10 nM) (E: miR-21, F: miR-135b) in HEK293T cells. At 48 hr posttransfection, miRNA expression levels were analyzed with qRT-PCR.

(G) Upregulation of mature miRNA levels, but not pri-miRNA levels, of several miRNAs by MCPIP1 depletion. The levels of MCPIP1, pri-miRNAs, and mature miRNAs were compared by qRT-PCR analyses in HepG2 cells transfected with control siRNA or siRNA for *MCPIP1* (*$p < 0.05$, compared to Control siRNA; n = 3).

(H) Global effects of MCPIP1 knockdown on endogenous miRNA expression, analyzed by miRNA microarray analysis in HepG2 cells. The proportion of miRNAs at different fold change levels is shown in the right panel. See also Figure S2. Error bars represent SEM.

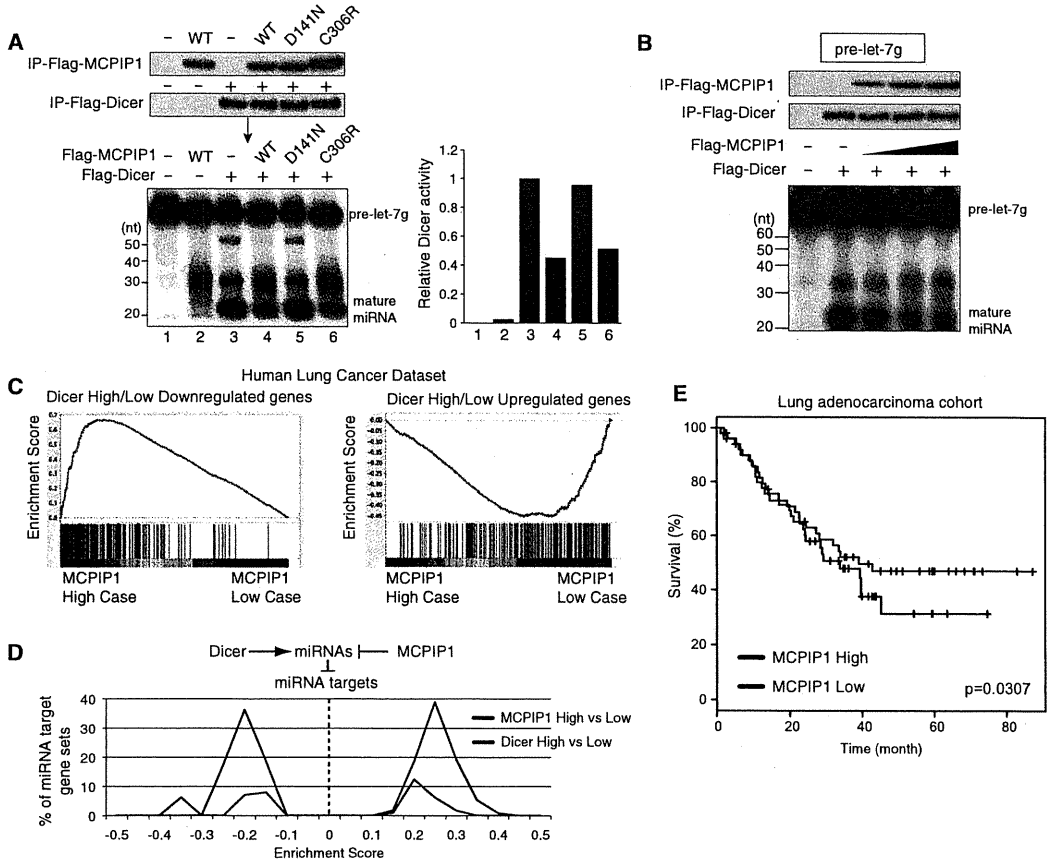

Figure 4. Antagonism between MCPIP1 Ribonuclease and Dicer and Its Implication in Human Cancer

(A and B) In vitro competition analysis using FLAG-Dicer, FLAG-MCPIP1 mutants (A), or increased amounts of FLAG-MCPIP1 (B) and radiolabeled pre-let-7g. Cleaved mature miRNAs are quantified as relative Dicer activity (A, right).

(C) Gene set enrichment analysis (GSEA) for genes negatively or positively associated with Dicer expression ("Dicer High/Low Downregulated or Upregulated genes"), along with the patients with high and low MCPIP1 expression ("MCPIP1 High Case" versus "MCPIP Low Case"), in the cohort of lung adenocarcinoma patients (Bild et al., 2006). Genes negatively or positively associated with Dicer expression were enriched in MCPIP1-High group and MCPIP1-Low group, respectively.

(D) Global histogram showing distribution of GSEA enrichment scores for the putative miRNA target gene sets in the lung adenocarcinoma cohort (Bild et al., 2006). In the comparison between Dicer-High and -Low groups, large proportion of miRNA target gene sets were underrepresented in Dicer-High group. In contrast, opposite asymmetrical distribution was observed in the comparison according to MCPIP1 expression, supporting the antagonism between Dicer and MCPIP1.

(E) Kaplan-Meier plots representing the survival probability in the same dataset, according to low or high MCPIP1 expression levels. The log-rank test p value reflects the significance of the association between high MCPIP1 expression and poor prognosis. See also Figure S4.

cleavage by MCPIP1 in vitro (Figure 6D), strengthening the importance of terminal loop as a target of MCPIP1.

While MCPIP1 has recently been shown to promote the mRNA decay of IL-6 (Matsushita et al., 2009), we noticed that the target element of IL-6 3′ UTR forms a stem-loop structure similar to pre-miRNAs (Matsushita et al., 2009; Paschoud et al., 2006) (Figure 6C, right). We similarly cloned the IL-6 3′ UTR fragments cleaved by MCPIP1 in vitro, and found that the ends of recovered 5′ and 3′ fragments were distributed in 5′- and 3′-franking regions of the hairpin structure, respectively (Figure S6D), supporting the idea that MCPIP1 preferentially targets the hairpin structure. We then investigated structural features of MCPIP1 target RNAs by generating a range of pre-miRNA mutants with various lengths of stem and terminal loop. As a result, deletion analysis showed that MCPIP1 could cleave pre-miRNA mutants with various stem lengths (Figures 6E and S6E), while deletion of the loop region affected MCPIP1 action in vitro, and MCPIP1 could not cleave pre-miRNA mutants without a loop region (Figures 6F and S6F, see d5–7 mutants). These findings thus suggest that MCPIP1 potentially controls the destinies of various hairpin RNAs. This notion parallels the finding that the Drosha-DGCR8 complex cleaves the hairpin structure in DGCR8 mRNA, as well as pri-miRNAs (Han et al., 2009). These observations imply the presence of dynamic crosstalk between the pathways for mRNA stability control and miRNA biogenesis.

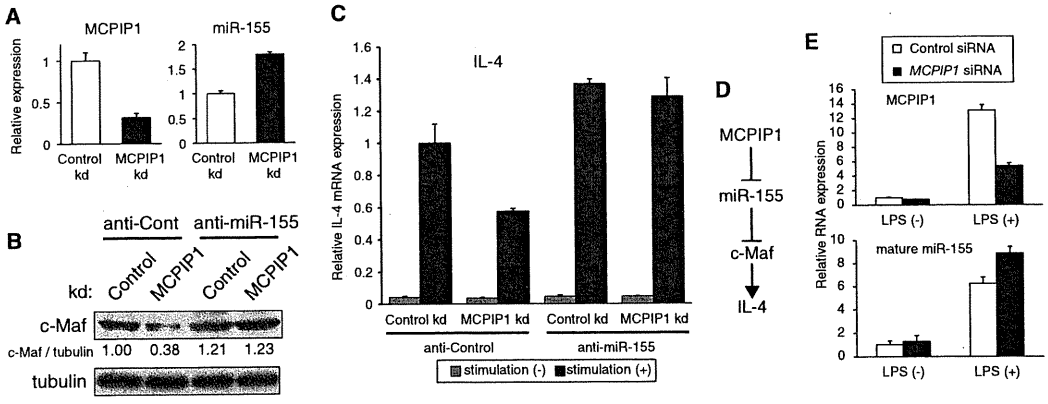

Figure 5. Modulation of miR-155/c-Maf Axis by MCPIP1

(A) miR-155 upregulation by MCPIP1 knockdown in Jurkat cells. Jurkat cells were transduced with MCPIP1 knockdown lentivirus vector (MCPIP1 kd) and analyzed by qRT-PCR analysis.

(B) miR-155-dependent c-Maf suppression by MCPIP1 depletion, as assessed by immunoblot analysis of c-Maf under a combination of MCPIP1 knockdown and transfection of anti-miR-155 inhibitor in Jurkat cells.

(C) Effects of MCPIP1 and miR-155 suppression on IL-4 induction by stimulation with PMA and ionomycin. Jurkat cells were prepared in the same combination as in (B) and analyzed by qRT-PCR analysis.

(D) Relationship of MCPIP1/miR-155/c-Maf/IL-4 axis.

(E) Involvement of MCPIP1 in LPS-mediated miR-155 upregulation in THP-1 macrophage cells, as assessed by qRT-PCR analysis after transfection with control siRNA or *MCPIP1* siRNA. See also Figure S5. Error bars represent SEM.

Oligomerization of MCPIP1 Ribonuclease via the Vertebrate-Specific C Terminus

In our study, other MCPIP family proteins (MCPIP2, MCPIP3, and MCPIP4) showed little effect on miRNA activity in spite of the presence of the conserved NYN domain and CCCH motif (Figures 1A, 7A, and S7A). Together with the differential effects of C306R mutation on in vitro and in vivo activities of MCPIP1 (Figures 3D–3G), these observations raised the possibility that other domain(s) including CCCH motif, besides the NYN domain, could be important for the in vivo function of MCPIP1. Besides the NYN domain, the CCCH zinc-finger domain and proline rich domain are placed at the central region and C-terminal region of MCPIP1, respectively (Figure 7A). In *C. elegans* and *Drosophila*, a similar protein with MCPIP1, C30F12.1 and CG10889, respectively, is observed (Figure 7A). These molecules lack a proline-rich domain found in MCPIP1 C terminus, and the C terminus of vertebrate MCPIP2/3/4 also shows little similarity with the MCPIP1 C terminus, suggesting that the C terminus of MCPIP1 has emerged as a certain functional domain in the vertebrate MCPIP gene family (Figure 7A).

Previous studies have demonstrated that some RNases and RNase domains, including RNase A and RNase L, function in the oligomerized state (Bergdoll et al., 1997; Salehzada et al., 1993). RNase A has been shown to oligomerize via a proline-dependent arm exchange mechanism (Bergdoll et al., 1997). Dicer has also been shown to function through intramolecular dimerization of its two RNase III domains (Zhang et al., 2004).

On the basis of these findings, we examined the possibility of MCPIP1 oligomerization via the unconserved C-terminal region including the proline-rich domain. While human MCPIP1 was usually observed as a 66 kDa monomer, the protein was detected as a high molecular weight complex of about 200 kDa under chemical crosslinking by disuccinimidyl suberate (DSS) (Figure 7B). Blue native PAGE analysis revealed that overexpressed and endogenous MCPIP1 proteins mainly exist as complexes of about 200 kDa, and of about 220 kDa and 600–700 kDa, respectively (Figure 7C). Immunoprecipitation analysis also detected an additional band of FLAG-tagged MCPIP1 with about 400 kDa in blue native PAGE (Figure 7D). Since these FLAG-MCPIP1 complexes were coimmunoprecipitated with cointroduced HA-tagged MCPIP1 (Figures 7B and 7D), these complexes may represent oligomeric forms of MCPIP1. In addition, endogenous MCPIP1 complexes of about 220 kDa and 600–700 kDa showed higher molecular weights than two FLAG-tagged MCPIP1 complexes of 200 kDa and 400 kDa, suggesting the presence of additional partner protein(s) interacting with endogenous MCPIP1. The conventional immunoprecipitation experiments confirmed the association between FLAG-tagged and HA-tagged MCPIP1 molecules (Figure S7B) and revealed that this oligomerization required the C-terminal region (Figures S7C and S7E). In accordance with the results, these C-terminal deletion mutants also showed reduced miRNA suppressor activities (Figures 7F, 7G, S7D, and S7E). Furthermore, RNA immunoprecipitation analysis clarified that both the CCCH motif and vertebrate-specific C terminus are important for efficient interaction between MCPIP1 and pre-miRNA in vivo, although the NYN domain has a minor role in this aspect (Figure 7H). We further observed that D141N and C306R mutants showed little dominant-negative effects on the function of wild-type MCPIP1 both in vivo and in vitro (Figure S7F). Collectively, MCPIP1 harbors several functional domains to inhibit miRNA maturation efficiently (Figure 7I). The presence of the vertebrate-specific MCPIP1 C terminus suggests that the

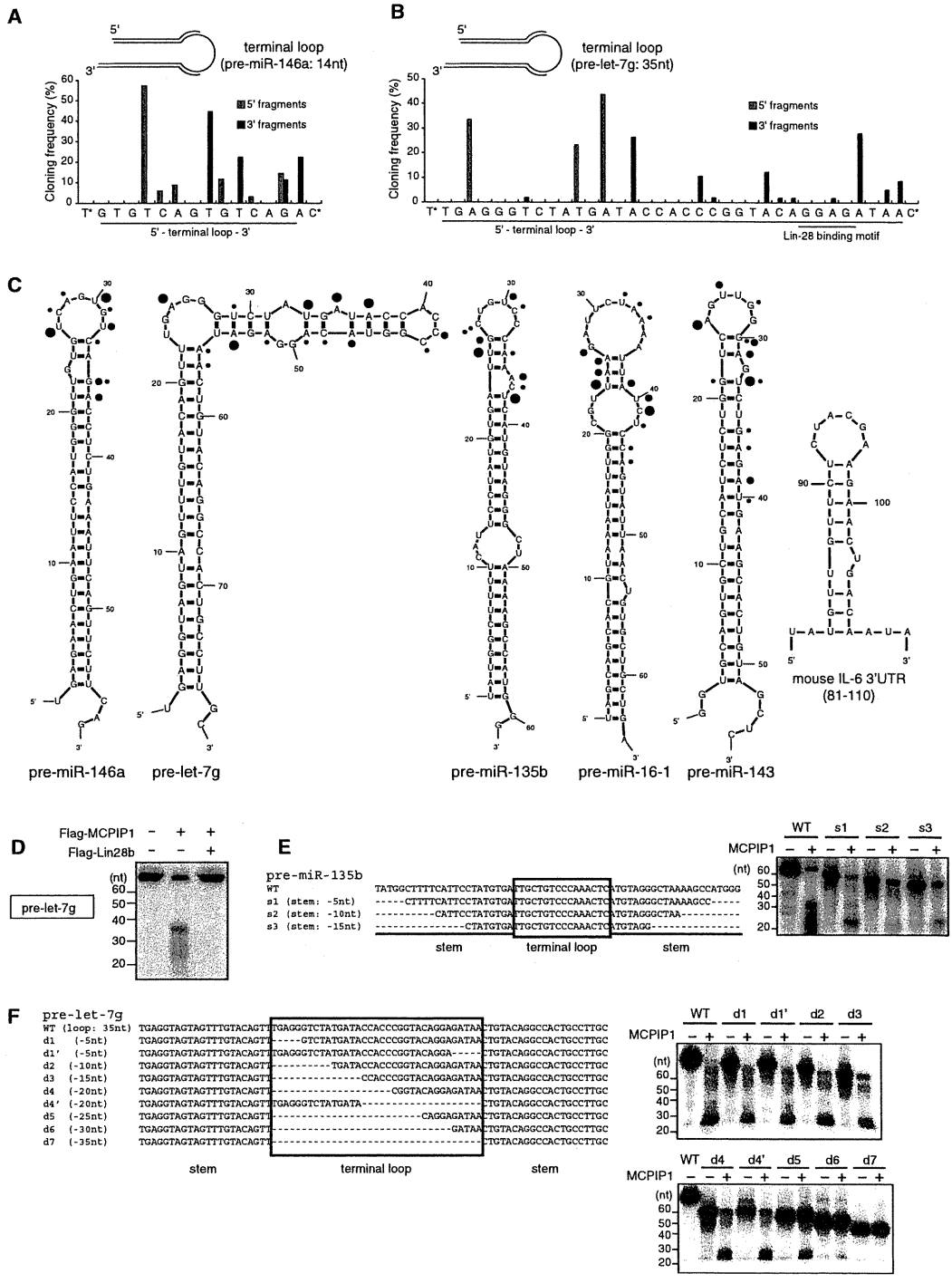

Figure 6. Targeting of the Terminal Loops of Pre-miRNAs by MCPIP1 Ribonuclease

(A and B) Cloning analysis of MCPIP1-cleaved pre-miRNA fragments. After in vitro cleavage reaction (90 min), the cleaved fragments of pre-miR-146a (A) and pre-let-7g (B) were cloned and sequenced. 5′ and 3′ fragments indicate the fragments composed of 5′ and 3′ mature miRNA strand and additional bases within the terminal loop, respectively. The data about pre-miR-135b, pre-miR-143, and pre-miR-16-1 are shown in Figures S6A–S6C.

(C) Comparison of the sequence analyses of MCPIP1-cleaved fragments (A and B and Figures S6A–S6C) and secondary structure prediction (Zuker, 2003). The ends of 5′ and 3′ fragments are indicated by blue and red circles, respectively. The structure of MCPIP1 target sequence of mouse *Il6* 3′ UTR (80–110) is also shown.

MCPIP family has evolved an anti-miRNA function of MCPIP1 in vertebrates.

DISCUSSION

Here we identified the CCCH zinc-finger ribonuclease MCPIP1 as an important RNase, which counteracts the productive miRNA biogenesis directed by two RNases, Drosha and Dicer (Figure 7J). It is poorly understood how the half-lives and absolute levels of mature miRNAs are determined, in comparison with advances concerning the mechanisms of miRNA production. Recent reports revealed that several nucleases, such as SDN in *Arabidopsis* and XRN-2 in *C. elegans*, degrade mature miRNAs (Chatterjee and Grosshans, 2009; Ramachandran and Chen, 2008). The present study first demonstrated that not only mature miRNAs but also pre-miRNAs are targets of active degradation to reduce miRNA activities. Considering that MCPIP1 expression dynamically changes during the inflammatory response (Liang et al., 2008a; Liang et al., 2008b), the rate of de novo miRNA synthesis might be actively regulated through the pre-miRNA decay by MCPIP1. Accordingly, global downregulation of miRNAs including miR-16 (as also demonstrated in Figure S5C) and overall shortening of mRNA 3′ UTRs have been observed along T cell activation (Sandberg et al., 2008; Wu et al., 2007).

Open questions remain regarding how MCPIP1 recognizes pre-miRNAs and preferentially inhibits the miRNA pathway and whether MCPIP1 uniformly acts on individual miRNAs. While further investigation is important, our trial analysis of RNA-IP/sequencing experiments suggested that the MCPIP1 D141N mutant interacts with a range of miRNA precursors and transcripts including IL6 (Figures S7G and S7H). On the other hand, the expression levels of externally expressed DGCR8 mRNA and IL-6 3′ UTR RNA both containing a hairpin structure decreased to about 50% by MCPIP1 overexpression (Figure S7I, left), as well as pre-miRNAs, but MCPIP1 knockdown only slightly upregulated the endogenous DGCR8 and IL-6 mRNA levels and also failed to show significant or consistent effects on other RNA species such as Alu and tRNAs (Figure S7I, right), in contrast to the effects on endogenous mature miRNAs. Considering that MCPIP1 decreased overexpressed pre-miRNAs by about half and their mature forms by about one-tenth (Figure 1), these results suggest that the miRNA biogenesis pathway is more susceptible to MCPIP1 regulation than other RNA species, maybe because of the requirement for stepwise collaboration of multiple maturation processes. Differential localization of MCPIP1 and various RNA species may also contribute to the strong inhibitory impact of MCPIP1 on the miRNA pathway. In addition, heterogenous effects of MCPIP1 knockdown on individual mature miRNAs (Figures 2G and 2H) might be attributable to intrinsic properties of MCPIP1, as influenced by preferential target structures/sequences and additional partner protein(s), or complexity of regulation of each miRNA modified by various factors, including pri-miRNA transcription, Drosha processing, cytoplasmic export, Dicer processing, existence of specific RNA-binding proteins, and miRNA stability regulation.

Lin-28 interacts with the terminal loop of let-7 precursor and specifically hinders let-7 maturation. In addition, several other RNA-binding proteins such as hnRNP A1 and KSRP also interact with the terminal loops of miRNA precursors and rather facilitate the processing of pri-miRNAs and/or pre-miRNAs. Considering that MCPIP1 targets the terminal loop of pre-miRNAs, these RNA-binding proteins might protect miRNA precursors from the degradation in addition to their intrinsic function in miRNA biosynthesis. Since the loop region is largely considered dispensable for the basic action of Drosha and Dicer, the evolutionarily conserved loops of many miRNA precursors might contain regulatory information for active degradation to differentially generate distinct miRNA species.

Our results demonstrated the importance of the C terminus for MCPIP1 function and its poor conservation between invertebrates and vertebrates (Figure 7). These findings suggest that the vertebrate MCPIP family has diversified and evolved an anti-miRNA function of MCPIP1. Although miRNA and RNAi pathways and their components are well conserved across a wide range of species, previous studies suggested certain evolutional differences, in particular from immunological aspects, as represented by different major antiviral mechanisms between plants/invertebrates and mammals, i.e., respectively, RNAi response and interferon (IFN) response (Umbach and Cullen, 2009). In addition, miRNAs encoded in certain mammalian viruses perturb host gene regulatory networks and there exist several mechanisms represented by RNase L and ZAP to avoid the promiscuity by viral-derived RNA species in vertebrate cells (Sadler and Williams, 2008). The presence of MCPIP1-mediated abortive processing machinery and diversity of MCPIP1-related genes, taken together with these findings, may therefore imply dynamic evolutional transition of RNA silencing system.

In the present study, we have intriguingly found an inverse correlation between MCPIP1 and Dicer function in human lung cancer cohorts (Figures 4C–4E and S4). Importantly, we observed an association of high MCPIP1 expression with poor survival, suggesting the usefulness of MCPIP1 as a prognostic marker. MCPIP1 upregulation by several inflammatory stimuli, including MCP1, might be partly attributable to global miRNA downregulation in cancer, in addition to reduced expression of Dicer and/or Drosha and mutations in TRBP and XPO5. Future studies may provide useful information about involvement of MCPIP1 in miRNA dysregulation in human malignancies and important insights for the efficiency of RNA-based therapeutics. In conclusion, the present work provides a clue for the comprehensive understanding of miRNA dynamics during the

(D) Effect of Lin-28b addition on MCPIP1 activity targeting pre-let-7g.
(E) Effect of the stem length of pre-miRNA on MCPIP1 activity. (Left) The sequences of deletion mutants of pre-miR-135b with various lengths of stem region. (Right) In vitro cleavage assay by coincubation of radiolabeled pre-miR-135b mutants and FLAG-MCPIP1 for 90 min.
(F) Effect of the terminal-loop length of pre-miRNA on MCPIP1 activity. (Left) The sequences of deletion mutants of pre-let-7g carrying a long terminal loop (35 nt). (Right) In vitro cleavage assay by coincubation of radiolabeled pre-let-7g mutants and FLAG-MCPIP1 for 120 min. See also Figure S6.

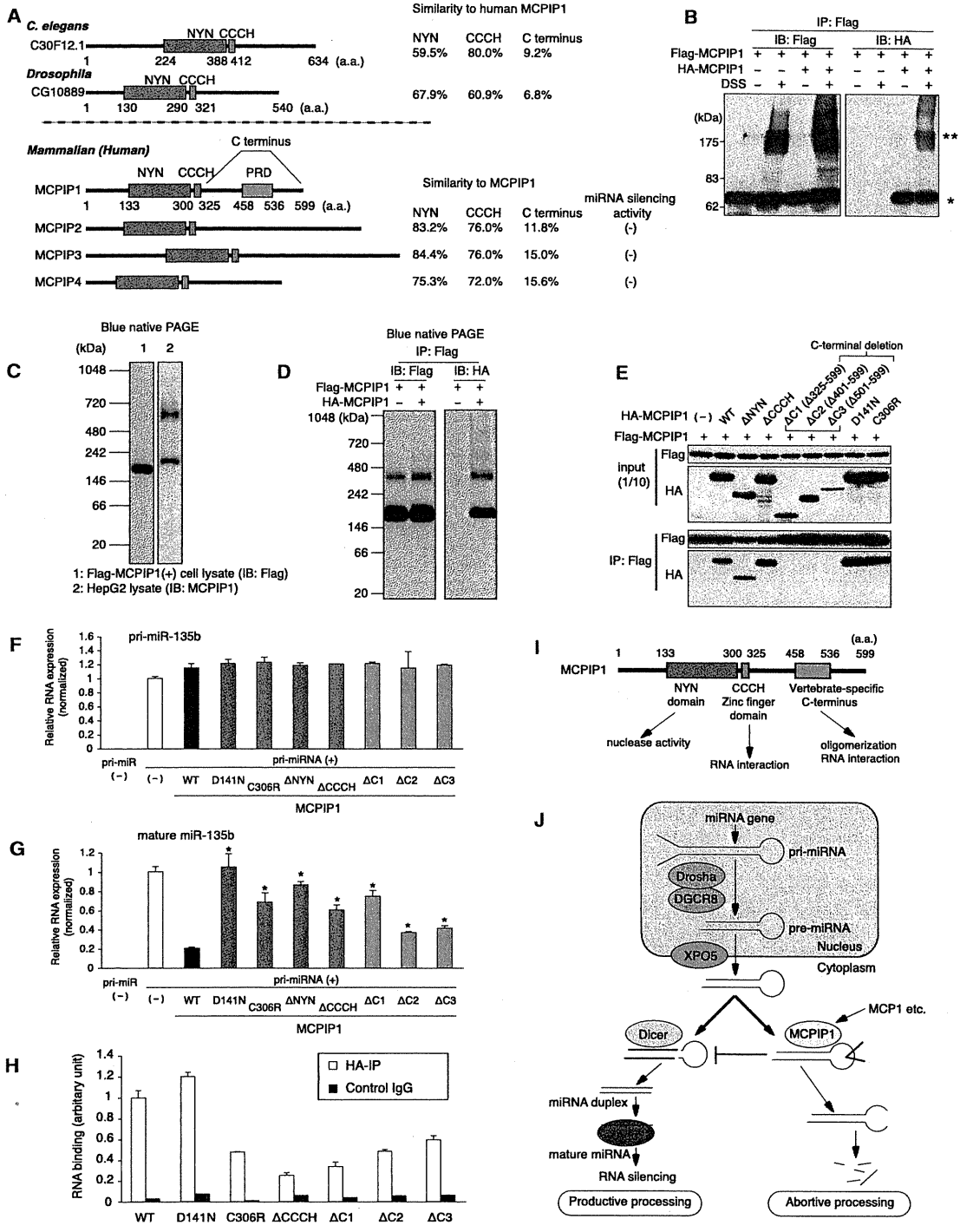

Figure 7. Oligomerization via Vertebrate-Specific C Terminus Is Important for miRNA Silencing Activity of MCPIP1

(A) Schematic representation of human MCPIP family proteins and invertebrate MCPIP1-related proteins (*C. elegans* C30F12.1 and *Drosophila* CG10889). The numbers on the right indicate the sequence similarity to human MCPIP1 protein.

(B) Oligomerization of MCPIP1. FLAG-MCPIP1 and HA-MCPIP1 were ectopically expressed in HEK293T cells. Cell lysates were crosslinked with DSS and immunoprecipitated with the anti-FLAG antibody followed by immunoblotting. Asterisks (*, **) indicate MCPIP1 monomers and oligomers, respectively.

physiological and pathological processes, such as inflammation and cancer.

EXPERIMENTAL PROCEDURES

Cell Lines, Antibodies, and Reagents

HEK293T, HepG2, Jurkat, and THP-1 cell lines were obtained from the American Type Culture Collection. HEK293T and HepG2 cells were maintained in Dulbecco's modified Eagle's medium (GIBCO) containing 10% fetal bovine serum (FBS). Hematological cell lines were maintained in RPMI1640 medium (GIBCO) with 10% FBS. Plasmids, antibodies, and reagents are described in the Supplemental Experimental Procedures.

Luciferase Reporter Assay, qRT-PCR Assays, and Northern Blot Analyses

Dual renilla/luciferase assays, qRT-PCR assays, and northern blot analyses were carried out as previously described (Suzuki et al., 2009). The expression levels of mature miRNAs were determined using TaqMan MicroRNA assay kit (Applied Biosystems) according to the manufacturer's protocol. The primer sequences used and related procedures are described in the Supplemental Experimental Procedures.

Immunocytochemistry

Immunostaining was carried out with anti-HA antibody, followed by counterstaining with TOTO-3 (Invitrogen–Molecular Probes). Stained specimens were examined using a LSM 510 META confocal microscope (Carl Zeiss).

In Vitro Pre-miRNA Cleavage Assay

In vitro pre-miRNA cleavage assay was performed modifying the method of in vitro pri-miRNA processing assay described previously (Suzuki et al., 2009). α^{32}P-UTP-internally-labeled pre-miRNAs were generated by in vitro transcription using PCR fragments containing pre-miRNA sequences fused to a T7 RNA polymerase promoter as templates. The detailed procedures are described in the Supplemental Experimental Procedures.

Immunoprecipitation and Immunoblot assay

Cells were lysed with Nonidet P-40 lysis buffer and subjected to immunoblot assay with standard procedures.

Cloning of Pre-miRNA Fragments

MCPIP1-cleaved RNA fragments were cloned and sequenced using microRNA cloning kit (Wako) according to the manufacturer's instructions. Briefly, the fragments were isolated using Trizol (Invitrogen), after in vitro cleavage reaction (90 min) without radioisotope as described above. We ligated 3′ adaptors into the RNA fragments with thermostable ssDNA ligase (Wako). The ligated substrate was reverse-transcribed, ligated with 5′ adaptors, and further PCR-amplified using HOT Goldstar DNA Polymerase (Wako). The PCR products were cloned into pCR2.1-TOPO vectors (Invitrogen) and sequenced.

RNA Immunoprecipitation Assay

RNA immunoprecipitation assay was performed as previously described (Suzuki et al., 2009).

Gene Expression Profiling Analysis

Gene expression profiling data of lung cancer patients were previously described (in Bild et al., 2006 [Figures 4C–4E], Shedden et al., 2008 [Figures S4B and S4D], and Larsen et al., 2007 [Figures S4C and S4E]), and were obtained from caArray system or NCBI's Gene Expression Omnibus. The expression levels of Dicer or MCPIP1 were evaluated by the corresponding probes. GSEA was performed with GSEA software available from the Broad Institute (http://www.broadinstitute.org/gsea/) (Subramanian et al., 2005). GSEA-embedded potential miRNA target gene sets were used. Survival analysis was performed using the survival package of R, the survfit function and the survdiff function.

SUPPLEMENTAL INFORMATION

Supplemental Information includes seven figures and Supplemental Experimental Procedures and can be found with this article online at doi:10.1016/j.molcel.2011.09.012.

ACKNOWLEDGMENTS

We thank K. Isogaya, K. Horiguchi, D. Koinuma, and T. Watabe for discussion; M. Tanaka and T. Funakoshi (Wako) for technical advice; T. Yokochi for encouragement; and all members of the Department of Molecular Pathology, at the University of Tokyo. This work was supported by KAKENHI (Grant-in-Aid for Scientific Research for Research Activity start-up [No. 22890038] and on Innovative Areas "RNA regulation" [No. 23112702]), the Global Center of Excellence Program for "Integrative Life Science Based on the Study of Biosignaling Mechanisms" from the Ministry of Education, Culture, Sports, Science, and Technology of Japan, and the Cell Science Research Foundation.

Received: March 4, 2011
Revised: June 17, 2011
Accepted: September 7, 2011
Published: November 3, 2011

REFERENCES

Anantharaman, V., and Aravind, L. (2006). The NYN domains: novel predicted RNAses with a PIN domain-like fold. RNA Biol. *3*, 18–27.

Bergdoll, M., Remy, M.H., Cagnon, C., Masson, J.M., and Dumas, P. (1997). Proline-dependent oligomerization with arm exchange. Structure *5*, 391–401.

Bild, A.H., Yao, G., Chang, J.T., Wang, Q., Potti, A., Chasse, D., Joshi, M.B., Harpole, D., Lancaster, J.M., Berchuck, A., et al. (2006). Oncogenic pathway signatures in human cancers as a guide to targeted therapies. Nature *439*, 353–357.

Chatterjee, S., and Grosshans, H. (2009). Active turnover modulates mature microRNA activity in Caenorhabditis elegans. Nature *461*, 546–549.

(C and D) Blue native PAGE analyses. HEK293T cells expressing FLAG-MCPIP1 or HepG2 cells were subjected to blue native PAGE analysis using FLAG antibody or MCPIP1 antibody (C). FLAG immunoprecipitates from cell lysates containing FLAG-MCPIP1 and HA-MCPIP1 were also analyzed by blue native PAGE analysis after elution with FLAG peptide (D).
(E) Requirement of the C terminus for MCPIP1 oligomerization. FLAG-MCPIP1 and HA-MCPIP1 mutants were ectopically expressed in HEK293T cells. Cell lysates were immunoprecipitated with the anti-FLAG antibody followed by immunoblotting.
(F and G) Effects of MCPIP1 mutation on miRNA maturation. MCPIP1 mutants were coexpressed with pri-miR-135b in HEK293T cells. At 48 hr posttransfection, the expression levels of pri-miRNA (F) and mature miRNA (G) were analyzed with qRT-PCR analyses (*$p < 0.05$, compared to wild-type MCPIP1 [WT]; n = 3).
(H) pre-miRNA binding capacity of MCPIP1 mutants. HEK293T cells were cotransfected with pri-miR-135b expression vector and various MCPIP1 mutant expression vectors. After transfection, MCPIP1 mutants were immunoprecipitated with anti-HA antibody and subjected to RT-PCR analysis with pre-miR-135b primers. As controls, RNA samples immunoprecipitated with nonspecific IgG (Control IgG; n = 3) were subjected to PCR.
(I) Differential contribution of MCPIP1 domains for miRNA silencing activity.
(J) A schematic model for the inhibition of miRNA processing by MCPIP1. See also Figure S7. Error bars represent SEM.